

Master's Thesis

Title

**Attractor Selection-based
Overlay Multipath Routing for Achieving Max-Min Fairness**

Supervisor

Professor Masayuki Murata

Author

Takahiro Inoue

February 15th, 2010

Department of Information Networking
Graduate School of Information Science and Technology
Osaka University

Attractor Selection-based
Overlay Multipath Routing for Achieving Max-Min Fairness

Takahiro Inoue

Abstract

To satisfy diverse requirements of users and applications, variety of application-oriented overlay networks are deployed over physical IP networks. Since these overlay networks share and compete for physical network resources such as routers and links, they interact and interfere with each other. Consequently, the quality of service of physical networks perceived by an overlay network dynamically changes for unpredictable internal and external causes. As far as overlay networks selfishly and independently behave, the overall performance easily deteriorates. In this paper, for multiple overlay networks to achieve more adaptive and stable performance in the shared environment, we propose a novel multipath routing mechanism. With our mechanism, each overlay network autonomously distributes traffic among available paths taking into account the load of paths, so that the max-min fairness in sharing network bandwidth among overlay networks can be achieved. For this purpose, we adopt a model of adaptive and autonomous behavior of biological systems, that is, the attractor selection model. In the attractor selection model, a biological system, e.g. bacteria, adapts its behavior such as metabolic synthesis to keep the activity or growth rate high in dynamically changing nutrient condition. By regarding multipath routing as metabolic synthesis, we can expect adaptive routing in dynamically changing load condition. We conduct simulation experiments where multiple overlay sessions having multiple available paths exist over a single physical network. Simulation results show that overlay networks fairly share the link bandwidth in a max-min fair manner with the average mean square error of 0.05, whereas there is neither centralized control nor global optimization. Overlay networks are also shown to be adaptive to dynamic changes in the network condition caused by injection of background traffic.

Keywords

Biologically-inspired

Overlay Network

Multipath Routing

Attractor selection

Max-Min Fairness

Contents

1	Introduction	8
2	Biological Models	11
2.1	Attractor Selection Model	11
2.2	Extended Attractor Selection Model	14
3	Overlay Multipath Routing based on Extended Attractor Selection Model	22
3.1	Application of Biological Model to Multipath Routing Algorithm	22
3.2	Implementation of Overlay Multipath Routing	26
4	Simulation	30
4.1	Simulation Setting	30
4.2	Simulation Results	33
5	Conclusion	60
	References	64
	Acknowledgements	64

List of Figures

1	Bacteria in reactor in attractor selection model	12
2	Dynamics of state of bacteria with high growth rate	12
3	Dynamics of state of bacteria with low growth rate	12
4	Dynamics of state of bacteria with increasing growth rate	13
5	Nutrient concentration in reactor	15
6	Nutrient concentration in bacteria	15
7	Growth rate of bacteria	16
8	Bacteria in reactor in extended attractor selection model	17
9	Concentration of nutrient i in reactor	20
10	Mean concentration of nutrient in bacterial cell i	21
11	Mean growth rates of bacterial cell producing nutrient i	21
12	Overlay session in network	23
13	Dynamics of the third term of Eq. (16)	25
14	Route setup by RREQ	27
15	RREQ forwarding	28
16	Replaying RREP by destination node	28
17	RREP forwarding	29
18	Topology of overlay network (Scenario 1 : single session)	31
19	Background traffic (Scenario 1 : single session)	32
20	Topology of overlay network (Scenarios 2 and 3 : two sessions)	33
21	Topology of overlay network (Scenario 4 : multiple session)	34
22	Acvitivity of micro traffic 1 (Scenario 1: single session)	35
23	Volume of micro traffic 1 (Scenario 1 : single session)	36
24	Utilization ratio of micro traffic 1 (Scenario 1 : single session)	36
25	Acvitivity of micro traffic 2 (Scenario 1 : single session)	37
26	Volume of micro traffic 2 (Scenario 1 : single session)	37
27	Utilization ratio of micro traffic 2 (Scenario 1 : single session)	38
28	Acvitivity of micro traffic 3 (Scenario 1 : single session)	38
29	Volume of micro traffic 3 (Scenario 1 : single session)	39

30	Utilization ratio of micro traffic 3 (Scenario 1 : single session)	39
31	Amount of traffic of overlay session (Scenario 1 : single session)	40
32	Activity of overlay session (Scenario 1 : single session)	40
33	Volume of micro traffic 1 of overlay session 1 (Scenario 2 : two sessions) . .	41
34	Utilization ratio of micro traffic 1 of overlay session 1 (Scenario 2 : two sessions)	42
35	Volume of micro traffic 2 of overlay session 1 (Scenario 2 : two sessions) . .	42
36	Utilization ratio of micro traffic 2 of overlay session 1 (Scenario 2 : two sessions)	43
37	Volume of micro traffic 1 of overlay session 2 (Scenario 2 : two sessions) . .	43
38	Utilization ratio of micro traffic 1 of overlay session 2 (Scenario 2 : two sessions)	44
39	Volume of micro traffic 2 of overlay session 2 (Scenario 2 : two sessions) . .	44
40	Utilization ratio of micro traffic 2 of overlay session 2 (Scenario 2 : two sessions)	45
41	Amount of traffic on overlay path 1 (Scenario 2 : two sessions)	45
42	Amount of traffic of each overlay sessions (Scenario 2 : two sessions)	46
43	Volume of micro traffic 1 of overlay session 1 (Scenario 3 : two sessions) . .	47
44	Utilization ratio of micro traffic 1 of overlay session 1 (Scenario 3 : two sessions)	48
45	Volume of micro traffic 2 of overlay session 1 (Scenario 3 : two sessions) . .	48
46	Utilization ratio of micro traffic 2 of overlay session 1 (Scenario 3 : two sessions)	49
47	Volume of micro traffic 1 of overlay session 2 (Scenario 3 : two sessions) . .	49
48	Utilization ratio of micro traffic 1 of overlay session 2 (Scenario 3 : two sessions)	50
49	Volume of micro traffic 2 of overlay session 2 (Scenario 3 : two sessions) . .	50
50	Utilization ratio of micro traffic 2 of overlay session 2 (Scenario 3 : two sessions)	51
51	Amount of traffic on overlay path 0 (Scenario 3 : two sessions)	51
52	Amount of traffic of each overlay sessions (Scenario 3 : two sessions)	52

53	Amount of total traffic of each overlay session (Scenario4 : 10 sessions) . . .	52
54	Amount of traffic of overlay sessions 1 (Scenario4 : 10 sessions)	53
55	Amount of traffic of overlay sessions 2 (Scenario4 : 10 sessions)	53
56	Amount of traffic of overlay sessions 3 (Scenario4 : 10 sessions)	54
57	Amount of traffic of overlay sessions 4 (Scenario4 : 10 sessions)	54
58	Amount of traffic of overlay sessions 5 (Scenario4 : 10 sessions)	55
59	Amount of traffic of overlay sessions 6 (Scenario4 : 10 sessions)	56
60	Amount of traffic of overlay sessions 7 (Scenario4 : 10 sessions)	56
61	Amount of traffic of overlay sessions 8 (Scenario4 : 10 sessions)	57
62	Amount of traffic of overlay sessions 9 (Scenario4 : 10 sessions)	57
63	Amount of traffic of overlay sessions 10 (Scenario4 : 10 sessions)	58
64	Average MSE against different coefficient T_{lim}	58
65	Mean convergence time against different coefficient T_{lim}	59

List of Tables

1	Parameters used in simulation of attractor selection model	16
2	Parameters used in simulation of extended attractor selection model	20
3	Parameters (All scenario)	31
4	Parameters used in the simulation (Scenario 4 : multiple session)	33
5	Comparison of average traffic to optimal traffic	60

1 Introduction

Many overlay networks are deployed in the Internet to satisfy diverse requirements of a variety of applications and various network services, which are beyond basic functionality of the Internet. For example, content distribution networks (CDN) such as Akamai [1] usually construct overlay networks for multicasting [2], since the current Internet does not support IP multicast services globally. Overlay routing is another example of applications of overlay network technologies and one of popular research areas [3, 4, 5, 6]. In the Internet, an underlying IP network provides an end-to-end session with a hop-count based shortest path only, where the physical link cost is given as one or an inverse of link capacity. As new applications emerge, a need arises for communication paths satisfying other QoS (Quality of Service), such as bandwidth for video streaming, delay for real-time applications such as video conferencing, and other attributes, e.g. stability, availability, and robustness. By using overlay network technologies, routing can take into account a variety of network characteristics in finding and establishing a path which satisfies various QoS requirements of an application, whereas an overlay link between a pair of overlay nodes is still governed by physical routing mechanisms.

However, it should be noted that physical network resources such as link bandwidth and processing and buffering capacity of routers are shared among overlay networks. If they compete for the limited physical resources in a selfish manner to pursue their own benefit and maximize their utility, they disrupt each other and it leads to degradation of the whole performance. Several papers [7, 8, 9, 10, 11, 12] analyzed such harmful interactions and showed that selfish routing led to the instability of a system, degraded performance of competing overlay networks, and made traffic engineering meaningless. An example of such harmful interactions is that a change an overlay path in an overlay network to avoid a congested link affects the performance of other overlay networks sharing the same physical network resources and it causes chains of reactions.

In these papers, they not only pointed out the problem, but also proposed mechanisms to solve the problem. For example, [7] makes suggestions to improve the overall stability of the system by imposing some restraints, e.g. randomization. The problem of competition becomes more harmful and becomes difficult to resolve when we consider overlay multipath

routing. For example, [13] proposes a game-theory based framework to resolve competition and maximize the global utilization. However, it requires the global view of the whole network to be provided to overlay networks and thus suffers from the scalability issue.

In this thesis, we propose a cooperative multipath routing for overlay networks where each overlay network autonomously distributes traffic among multiple paths. For this purpose, our proposal is based on our previous work on overlay multipath routing and extends it to accomplish the fair share of bandwidth. Our research group proposed an overlay multipath routing mechanism for adaptive and stable route selection under dynamically changing traffic condition [14]. The proposal there was based on a nonlinear mathematical model, called the attractor selection model. The attractor selection model imitates adaptive behavior of biological systems, e.g. bacteria, which adaptively adjust the rate of nutrient synthesis to keep alive and growing in dynamically changing nutrient condition. By regarding bacteria as overlay networks, selection of nutrient to synthesize as selection of path to use, and the growth rate as the performance, the proposed mechanism can achieve adaptive and stable multipath routing. Although in [14] we considered the behavior of only single overlay network, we believe that cooperative behavior emerges through interaction among overlay networks, each of which reacts to dynamically changing network condition. However, the process of emergence is unpredictable and uncontrollable and as such the resultant condition could be unfair in a viewpoint of sharing bandwidth.

Therefore, in this thesis, we first extend the attractor selection model to model competition among overlay networks for bandwidth. The extension is based on symbiotic behavior of bacteria in a reactor [15]. In the model of symbiosis of closely-related species of bacteria, bacteria indirectly interact with each other by permeation of metabolites through cell membrane. Metabolites diffuse through the cell membrane from and to the reactor in accordance with difference in metabolic concentrations in the cell and the reactor. The metabolic concentrations in the reactor correspond to traffic condition of logical links in overlay multipath routing. With our proposal, a sender of an overlay network autonomously determines the amount of traffic to send and distributes the traffic among multiple paths available between sender and receiver. As a result of autonomous behavior of overlay networks and interaction among them through competition for shared physical resources, the network bandwidth is well utilized and shared among overlay networks in

the max-min fair manner.

We conduct simulation experiments where multiple overlay sessions having multiple available paths exist over a single physical network. We first evaluate the adaptability of multipath routing by injecting background traffic to the network. Then, we evaluate how the max-min fairness is achieved among multiple overlay sessions.

The rest of the paper is organized as follow. In Sect. 2, we introduce the mathematical model of biological adaptation which our multipath routing is based on. Next in Sect. 3, we propose a multipath routing mechanism based on the extended attractor selection model. In Sect. 4, we evaluates the behavior of our multipath routing through simulation experiments. Finally, we summarize this paper and explain future directions in Sect. 5.

2 Biological Models

In this section, we explain the attractor selection model for adaptive nutrient synthesis of bacteria and the extended attractor selection model which additionally models symbiosis of bacteria in the shared environment.

2.1 Attractor Selection Model

The attractor selection model is a model of adaptive behavior of biological systems [16]. An attractor is a stable state of a dynamic system where a system converges after transition from the initial state. Bacteria, i.e. *E.coli* cells have a metabolic pathway, that is a network of chemical reaction in metabolic synthesis, to synthesize two different nutrients. Since chemical reactions of two nutrients are in the relation of mutual inhibition, a bacterial cell generates either of the two nutrients at a time. When the environment contains sufficient amount of both nutrients, a cell can live independently of which nutrient it produces. Once the environmental nutrient condition changes, for example, to lack of one nutrient, a cell autonomously and adaptively begins to produce the lacking nutrient to keep alive and growing. Although bacteria show such autonomous and adaptive behavior, there is no pre-programmed rule such as a signal transduction pathway. Instead, adaptation is driven by biological noise.

Figure 1 illustrates the condition where a bacteria cell is in a reactor whose culture media contains two kinds of nutrients necessary for growth of bacteria. Nutrients permeate the membrane and are used by bacteria to grow. Now, consider the concentrations of nutrients in a cell, denoted as m_1 and m_2 for nutrient type 1 and 2, respectively. The dynamics of nutrient concentrations is formulated as,

$$\frac{dm_1}{dt} = \frac{syn(\alpha)}{1 + m_2^2} - deg(\alpha)m_1 + \eta_1 \quad (1)$$

$$\frac{dm_2}{dt} = \frac{syn(\alpha)}{1 + m_1^2} - deg(\alpha)m_2 + \eta_2 \quad (2)$$

where α corresponds to the growth rate of bacteria, $syn(\alpha)$ and $deg(\alpha)$ are the rate coefficient of synthesis and decomposition, respectively and η_1 and η_2 are the white Gaussian noise as internal and external noise that affects the nutrient concentrations.

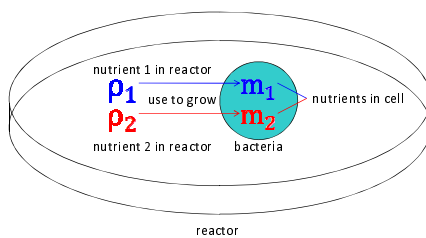


Figure 1: Bacteria in reactor in attractor selection model

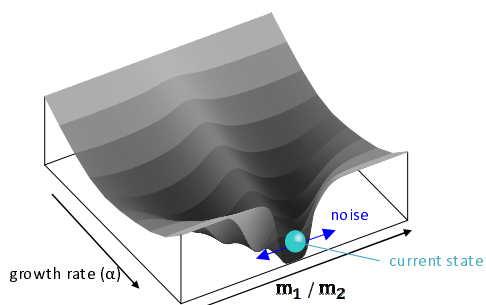


Figure 2: Dynamics of state of bacteria with high growth rate

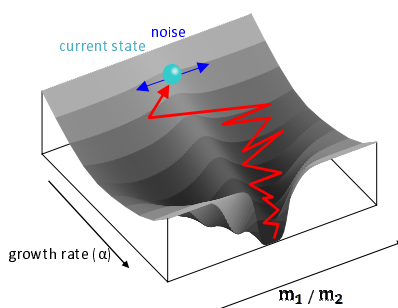


Figure 3: Dynamics of state of bacteria with low growth rate

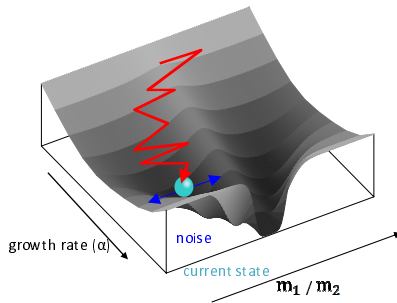


Figure 4: Dynamics of state of bacteria with increasing growth rate

Bacteria's growth rate α changes in accordance with nutrient concentrations in the cell and the reactor as,

$$\frac{d\alpha}{dt} = \frac{prod}{\left(\left(\frac{threshold_1}{m_1 + \rho_1}\right)^{n_1} + 1\right) \times \left(\left(\frac{threshold_2}{m_2 + \rho_2}\right)^{n_2} + 1\right)} - cons \times \alpha \quad (3)$$

where *prod* and *cons* are the rate coefficients of the production and consumption of nutrient, ρ_i is concentration of nutrient i in the reactor, and *threshold_i* and n_i define sensitivity of nutrient i .

The function *syn*(α) and *deg*(α) are given as, for example, ,

$$syn(\alpha) = \frac{6\alpha}{2 + \alpha} \quad (4)$$

$$deg(\alpha) = \alpha \quad (5)$$

When we consider this nonlinear dynamics without the noise terms, the dynamic system has an attractor $(m_1, m_2) = (m^*, m^*)$ with high activity α and attractors $(m^*, 1/m^*)$ and $(1/m^*, m^*)$ with low activity. Here, m^* is a constant.

In the attractor selection model, bacteria regulate synthesis rate of nutrients in accordance with dynamically changing nutrient condition in the environment. When the nutrient concentrations ρ_1 and ρ_2 are high enough in the reactor, the growth rate α of bacteria is high. Therefore, the influence of noise term in Eqs. (1) and (2) becomes small and the nutrient synthesis is dominated by the nonlinear dynamics defined by the first two terms in the right-hand side of the equations. Then, a bacteria cell stays at the attractor where concentrations m_1 and m_2 are at the same level (Fig. 2). When one of nutrients lacks from the reactor, growth rate α initially decreases. As a consequence, the dynamics

of bacteria becomes being driven by noise (Fig. 3). When a cell occasionally begins to synthesize the missing nutrient and the corresponding nutrient concentration increases, the growth rate eventually increases. Then, a cell is entrained to the attractor and stays there stably (Fig. 4). In this way, bacteria adaptively choose an attractor appropriate for the environmental condition.

Figures 5 through 7 show how bacteria adaptively select nutrient to produce by using simulation results. In these figures, the x-axis corresponds to simulation time and the y-axes show the nutrient concentrations ρ_1 and ρ_2 in the reactor, the nutrient concentrations m_1 and m_2 in a cell, and the growth rate α , respectively. Parameters used in the simulation are summarized in Table 1. At the beginning, the nutrient concentrations in the reactor are set at 3 as shown in Fig. 5, which are sufficient for the cell to grow as the high activity implies in Fig. 7. At this time, the nutrient concentrations in the cell are at the same level as shown in Fig. 6. Next at time 1000, nutrient 1 is cut off. Consequently, nutrient concentration ρ_1 decreases and the activity decreases as well. By being driven by noise, the cell eventually begins to synthesize nutrient 1 and the nutrient concentration m_1 increases at around 1100. Since this selection compensates the lack of nutrient 1 in the reactor, the growth rate is recovered to some extent at around 1100. Then, nutrient condition in the reactor changes for reinjection of nutrient 1 at time 2000. The cell reacts to this change and the nutrient synthesis becomes the same as the initial phase. Finally, nutrient 2 is cut off at time 3000, and the cell successfully changes its state to synthesize nutrient 2 and keeps it stably. Simulation results support the qualitative description of adaptive behavior.

2.2 Extended Attractor Selection Model

In a reactor, not only one, but many bacteria co-exist and their strains could be different from each other. The extended attractor selection model models symbiotic behavior of bacteria of closely related strains, where interaction among bacteria is formulated more explicitly. As with the attractor selection model, we consider two nutrients indispensable for growth of bacteria. Because of mutually inhibiting metabolic synthesis, a cell of bacteria can synthesize either of the two nutrients. Through permeation of membrane, nutrients diffuse between bacteria and the culture in the reactor (Fig. 8).

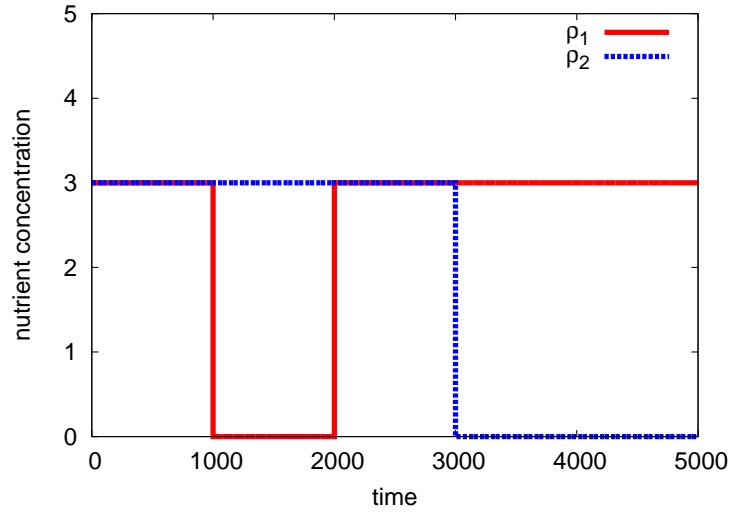


Figure 5: Nutrient concentration in reactor

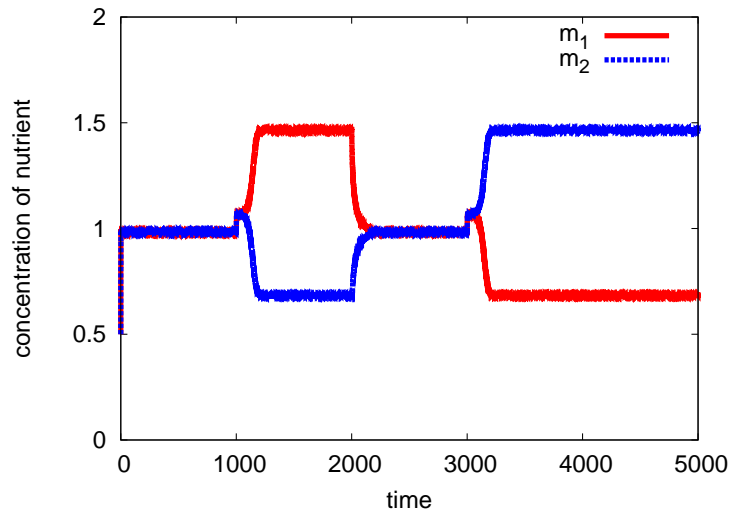


Figure 6: Nutrient concentration in bacteria

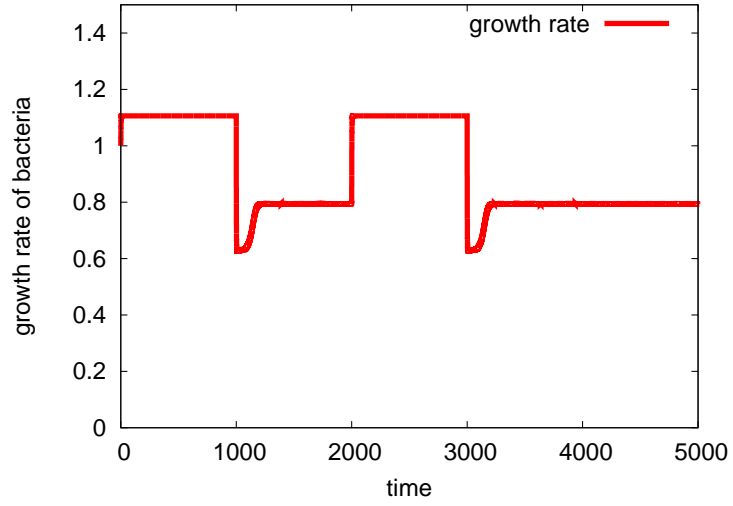


Figure 7: Growth rate of bacteria

Table 1: Parameters used in simulation of attractor selection model

mean of η_i	0
variance of η_i	0.01
initial nutrient concentration m_i	0.5
production coefficient $prod$	1
consumption coefficient $cons$	0.8
threshold $threshold_i$	1
exponent n_i	2

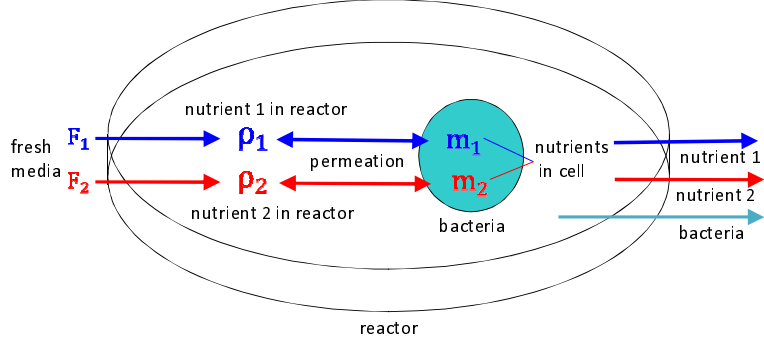


Figure 8: Bacteria in reactor in extended attractor selection model

Nutrient concentrations $xs1_i$ and $xs2_i$ of nutrient 1 and 2 in bacterial cell i change in accordance with the following nonlinear equations, respectively.

$$\frac{d}{dt}xs1_i = \mu_i \left(\frac{1}{1 + (xs2_i \times S)^2} - xs1_i \right) + \eta_1(t) \quad (6)$$

$$\frac{d}{dt}xs2_i = \mu_i \left(\frac{1}{1 + (xs1_i \times S)^2} - xs2_i \right) + \eta_2(t) \quad (7)$$

where μ_i is the growth rate of bacterial cell i , S is a coefficient of nutrient synthesis and defines the degree of suppression of synthesizing the other nutrient, and η is the white Gaussian noise. This nonlinear dynamics is similar to the one in the previous section.

The growth rate μ_i of bacterial cell i changes as,

$$\mu_i = \frac{1}{\left(1 + \frac{threshold_1}{\rho_1 + xs1_i - CON_1 \mu_i}\right)^2} \times \frac{1}{\left(1 + \frac{threshold_2}{\rho_2 + xs2_i - CON_2 \mu_i}\right)^2} \quad (8)$$

where ρ_1 and ρ_2 are concentrations of nutrients in the culture, and CON_1 and CON_2 are coefficients correspond to the consumption rate of nutrients for bacteria to grow, respectively. By Eq. (8), if concentrations of both nutrients are sufficient, the growth rate becomes 1.

Nutrient concentrations ρ_1 and ρ_2 in the culture changes for feeding and drain of fresh medium to the reactor and permeation. It is formulated as,

$$\frac{d}{dt}\rho_1 = D(F_1 - \rho_1) + \sum_{i=1}^N xv_i \times (xs1_i - CON_1 \mu_i) \quad (9)$$

$$\frac{d}{dt}\rho_2 = D(F_2 - \rho_2) + \sum_{i=1}^N xv_i \times (xs2_j - CON_2 \mu_i) \quad (10)$$

The fresh medium is supplied to the reactor and drains out from the reactor at the same rate, where we consider the chemostat cultivation. F_i ($i \in \{1, 2\}$) corresponds to the nutrient concentrations in the fresh medium fed into the reactor. D defines the dilution rate of the culture. Therefore, the first term of the right-hand side of the equations expresses temporal changes in the nutrient concentrations in the reactor for the chemostat cultivation. The second term takes into account nutrient exchanges with bacteria where xv_i indicates the volume of bacterial cell i , N is the number of bacteria in the reactor.

The volume xv_i of bacteria cell i changes in proportional to the growth rate μ_i .

$$\frac{d}{dt}xv_i = \mu_i \times xv_i \quad (11)$$

If the growth rate is high, the volume of a bacterial cell increases fast. When the volume becomes twice the size of initial volume, a bacterial cell undergoes cell division. The volume of each of new bacterial cells is the half of the original volume, which is identical to the initial volume of the cell. The nutrient concentrations and the growth rate are set at the same as the original cell. The number of bacterial cells decreases at the constant probability p . It means that a bacterial cell dies at the probability p at every time step or the ratio p of bacteria is taken out from the reactor at every time step.

Basically behavior of bacteria with the extended model is similar to that of the original attractor selection model, but bacteria show more interesting behavior because of mutual interaction. In Figs. 9 through 11, simulation results with a set of parameters summarized in Table 2 are shown. Figure 9 shows a time series of the nutrient concentrations ρ_1 and ρ_2 in the reactor. Figure 10 shows the average nutrient concentrations of bacteria. Figure 11 shows the average growth rate of bacteria, where "1 generator" indicates the average of bacteria whose $xs1_i > xs2_i$ and "2 generator" corresponds to the average of bacteria whose $xs1_i < xs2_i$. The nutrient concentrations F_1 and F_2 of fresh medium are both set at 2.0. At time 20, we stop feeding nutrient 1, that is, $F_1 = 0.0$. Since the initial nutrient concentrations in the reactor are sufficiently high (Fig. 9), bacteria suppress production of nutrients and thus the nutrient concentrations within bacteria decreases as shown in Fig. 10. Although the growth rate decreases to about 0.3 for this suppression in Fig. 11, it is high enough for bacteria to live and grow. In addition, thanks to plenty of nutrients, the growth rates are the same among bacteria independently of nutrient they synthesize.

At time 20, feeding of nutrient 1 is stopped. Then the concentration of nutrient 1 in the reactor suddenly decreases. Consequently, the growth rate of bacteria producing nutrient 2 drastically decreases, whereas the lack of nutrient also affects the growth rate of the other bacteria. Because of the low growth rate, bacteria producing nutrient 2 begin to be controlled by noise. Some of them occasionally changes the nutrient to synthesize from nutrient 2 to nutrient 1, and becomes "1 generator". Since the number of bacteria which synthesizes nutrient 1 gradually increases (not shown in figure), the concentration of nutrient 1 in bacteria shown in Fig. 10 eventually increases to compensate the lack of nutrient 1 in the reactor. Then, the growth rate recovers regarding "1 generator". At around time 40, the concentration of nutrient 1 in the reactor starts increasing for permeation from bacteria. It helps growth of "2 generator" and their growth rate also increases as shown in Fig. 11. However, because there is no mechanism to control or mediate adaptive behavior of bacteria, we observe the overshoot in nutrient generation. As many bacteria change their state to synthesize nutrient 1 more than nutrient 2, the concentration of nutrient 2 begins to decrease. Then, they suffer from lack of nutrient 2 and the growth rate of "1 generator" decreases. Because of low growth rate, some of them become "2 generator" by being driven by noise. Similarly, such adaptation causes the overshoot again. By repeating these processes, the condition of the system converges to the stable and balanced state.

Table 2: Parameters used in simulation of extended attractor selection model

mean of $\eta_i(t)$	0
variance of $\eta_i(t)$	0.01
initial number of bacteria	30
initial nutrient concentration of bacteria $xs1_i, xs2_i$	0.5
initial volume of bacteria v_i	0.01
coefficient of consumption rate of nutrient CON_i	1.4
initial nutrient concentration in reactor ρ_i	3.0
deletion rate p	0.3
synthesis coefficient S	10
threshold $threshold_i$	0.5
dilution rate D	0.3

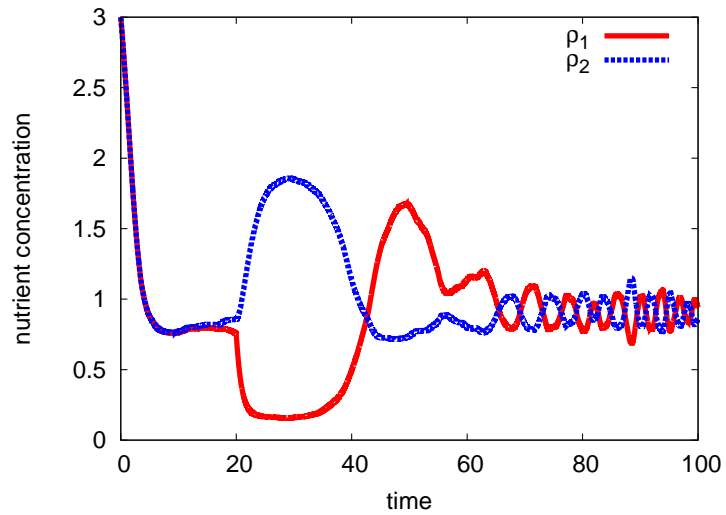


Figure 9: Concentration of nutrient i in reactor

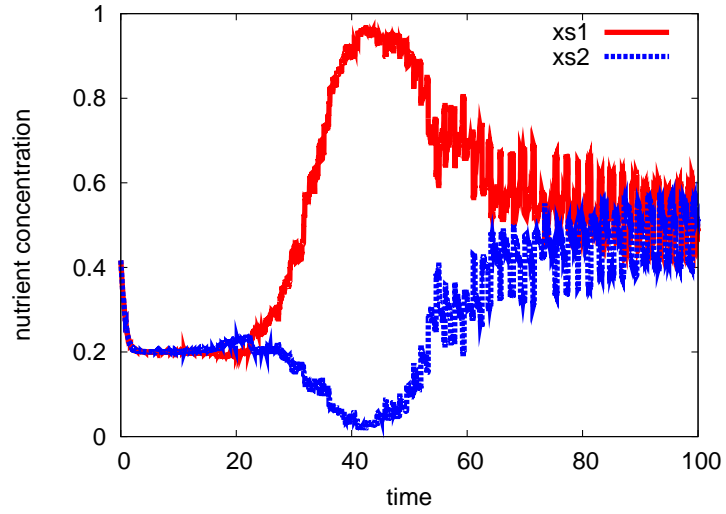


Figure 10: Mean concentration of nutrient in bacterial cell i

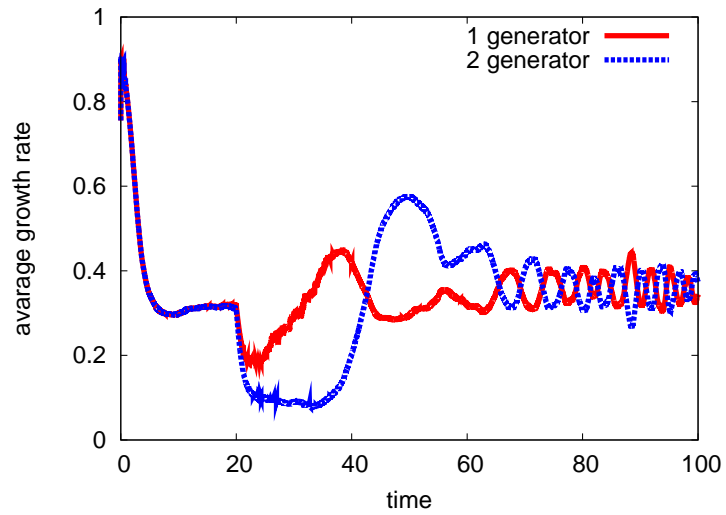


Figure 11: Mean growth rates of bacterial cell producing nutrient i

3 Overlay Multipath Routing based on Extended Attractor Selection Model

In this section we first propose a mathematical model to apply the extended attractor selection model to overlay multipath routing for the max-min fair share of bandwidth. Then we will explain how the model is adopted to overlay multipath routing in reality.

3.1 Application of Biological Model to Multipath Routing Algorithm

As in Fig. 12, we consider a scenario where multiple overlay paths are available for an overlay session whose source and destination nodes are overlay nodes. An overlay path consists of overlay links and each of overlay link consists of physical links. The way that a pair of overlay nodes at the ends of an overlay link depends on a routing mechanism employed in the physical network. Overlay paths do not need to be disjoint physically or logically. A source node of a session utilizes multiple paths by distributing traffic among them whereas it would happen that traffic occasionally is concentrated on a single path. There could exist multiple sessions among them physical and overlay links are shared. An overlay session is not aware of others. There is no way of direct or indirect communication among overlay sessions. We also assume that an overlay session can probe the load of each of overlay paths.

We regard the max-min fairness as the fair share of network bandwidth among multiple overlay sessions. The max-min fairness is the condition where no session can increase the amount of traffic, therefore, the bandwidth to use, on any of paths without forcing other sessions with the smaller amount of total traffic, i.e. sum of traffic that a session distributes over multiple paths, than itself under the constraints on the capacity of physical links.

In applying the extended attractor selection model to overlay multipath routing, we correspond the concentration of each nutrient in the reactor to the load of each overlay path, the concentration of each nutrient in a bacterial cell to the utilization ratio of each overlay path, the total volume of each bacterial cell to the total amount of traffic of each overlay session, and the growth rate to the degree of balance in load distribution among paths by each overlay session. By this mapping, an overlay session can dynamically and adaptively control the amount of traffic to distribute to each of multiple paths in

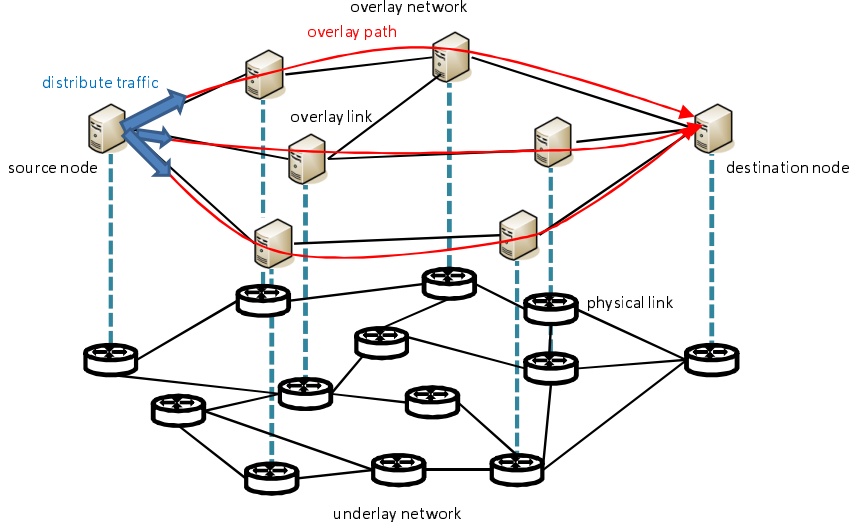


Figure 12: Overlay session in network

accordance with their load.

Based on the above assumption and mapping, a mathematical model of overlay multi-path routing is formulated as follows. Hereafter N corresponds to the number of overlay sessions and overlay session i ($1 \leq i \leq N$) has M_i overlay paths from a source to a destination.

The total amount of traffic that session i transmits is given as,

$$T_i = \sum_{j=1}^{L_i} v_{i,j} \quad (12)$$

where $v_{i,j}$ corresponds to the volume of so-called micro traffic, the virtual unit of traffic, which corresponds to a bacterial cell. The traffic of session i consists of the number L_i of micro traffic. $T_i(k)$ is the amount of traffic that session i allots to overlay path k ($1 \leq k \leq M_i$).

$$T_i(k) = \sum_{j=1}^{L_i} \left\{ v_{i,j} \frac{x_{i,j}(k)}{\sum_{l=1}^{M_i} x_{i,j}(l)} \right\} \quad (13)$$

where $x_{i,j}(k)$ corresponds to the utilization ratio of path k to send micro traffic j in overlay session i and $T_i = \sum_{k=1}^{M_i} T_i(k)$.

Session i distributes the volume $v_{i,j}$ of micro traffic j among overlay paths in proportional to utilization ratio $x_{i,j}(k)$. Utilization ratio $x_{i,j}(k)$ changes by the following

nonlinear equation,

$$\frac{d}{dt}x_{i,j}(k) = \mu_{i,j} \left[\frac{\mu_{i,j}}{1 + \{\max_{l \in M_i, l \neq k} x_{i,j}(l) \times S\}^2} - x_{i,j}(k) \right] + \eta_i(t) \quad (14)$$

where $\mu_{i,j}$ corresponds to the activity of micro traffic j in session i and S is a constant which show the degree of inhibition. Because of max operation, the dynamics expressed by Eq. (14) has M_i attractors, each of which has a large $x_{i,j}(k)$ for a certain k and small value for others. Therefore, one overlay path is preferentially chosen and mainly used by micro traffic j of overlay session i , when the activity $\mu_{i,j}$ is high.

The dynamics of activity $\mu_{i,j}$ of micro traffic j in overlay session i is formulated as

$$\mu_{i,j} = \frac{1}{\prod_{k=1}^{M_i} \left\{ 1 + \left(\frac{K}{\rho_i(k) + x_{i,j}(k) - C_i(k)\mu_{i,j}} \right)^2 \right\}} \quad (15)$$

where $C_i(k)$ is a coefficient which is determined in proportional to the minimum capacity of physical links that overlay path p of overlay session i traverses and K is sensitivity of load distribution. $\rho_i(k)$ is the load of overlay path k of overlay session i , which is the utilization or load of a physical link with the minimum capacity along the path, and $\rho_i(k)$ of 1 means full utilization. Eq. (15) implies that by allocating more traffic, i.e. larger $x_{i,j}(k)$, to less utilized path, i.e. smaller $\rho_i(k)$, the activity increases. That is, effective distribution of load over multiple paths can be accomplished.

The dynamics of volume $v_{i,j}$ of micro traffic j in overlay session i is formulated as

$$\frac{d}{dt}v_{i,j} = \mu_{i,j} \times v_{i,j} \times \left(\frac{2}{1 + \sum_{k=1}^{M_i} \frac{x_{i,j}(k)}{\sum_{l=1}^{M_i} x_{i,j}(l)} e^{-g(1-\rho_i(k))}} - 1 \right) \quad (16)$$

where g is a gain of the sigmoid function. For the biological model of extended attractor selection, chemostat cultivation is assumed. Thus, the number and the total volume of bacteria are controlled by injection of fresh medium to the reactor, discharge of culture containing bacteria from the reactor, and cell division. In multipath routing, to control the amount of traffic in accordance with the path capacity, which is identical to the minimum capacity of physical links constituting the path, the third term is added to Eq. (13) in Eq. (14). Figure 13 shows the function of the third term, where we assume there is only one path, i.e. $M_i = 1$, and $g = 10$. The x-axis corresponds to load $\rho_i(k)$ and the y-axis shows

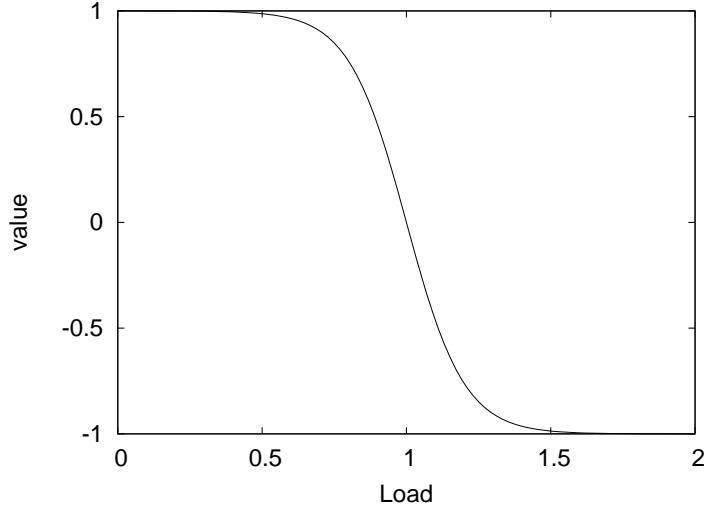


Figure 13: Dynamics of the third term of Eq. (16)

the value of the third term. As can be seen, when load $\rho_i(k)$ is close to 0 and path k is not loaded, volume $v_{i,j}$ increases as $\frac{dv_{i,j}}{dt} = \mu_{i,j} \times v_{i,j}$. When the path becomes loaded as $\rho_i(k)$ approaches to 1, the third term becomes smaller to suppress the increase of traffic volume. With $\rho_{i,j} = 0$, the traffic on the path stops increasing. As the load goes beyond 1 for some reasons, volume $v_{i,j}$ begins to decrease to solve the overloaded condition. Consequently, the amount of traffic on each path is controlled in accordance with the capacity of the path.

In the above mathematical model, each overlay session tries to distribute traffic among paths taking into account their load condition, to allocate more traffic to a less loaded path within the path capacity. However, this behavior alone cannot lead to the max-min fair share of network bandwidth among overlay sessions, since the rate of increase in the amount of traffic is proportional to the current traffic volume in Eq. (16). Consider a case that a physical link is shared by two sessions. One session, say session A, has already been using the link to the half of capacity, for example, when the other session B begins to use the link. Since volume $v_{A,j}$ of session A is larger than $v_{B,j}$, session A always occupies the link bandwidth more than session B even time passes. Here we further assume that the activity is the same among sessions. Then, the link becomes loaded and both sessions are forced to suppress traffic on the link by the third term of Eq. (16). Although the amount

of decrease is larger for session A than session B, it is also proportional to the traffic volume. Therefore, they never share the link bandwidth in a fair manner. This example implies that the total traffic should be taken into account in controlling the volume of traffic.

Then, Eq. (16) is rewritten as,

$$\frac{d}{dt}v_{i,j} = \mu_{i,j} \times v_{i,j} \times \sum_{k=1}^{M_i} \frac{x_{i,j}(k)}{\sum_{l=1}^{M_i} x_{i,j}(l)} \times S_{i,j}(k) \times I_{i,j} \quad (17)$$

$$S_{i,j}(k) = \begin{cases} 1 & (\rho_i(k) < 1) \\ -1 & (\rho_i(k) \geq 1) \end{cases} \quad (18)$$

$$I_{i,j} = \begin{cases} 1 - \frac{0.5}{1 + \frac{T_i}{T_{lim}}} & (\rho_i(k) \geq 1) \\ \frac{0.5}{1 + \frac{T_i}{T_{lim}}} & (\rho_i(k) < 1) \end{cases} \quad (19)$$

where $S_{i,j}(k)$ for micro traffic j on path k in session i is introduced in place of the sigmoid function-based control in Eq. (16) to switch between increase and decrease in accordance with the load condition $\rho_i(k)$ of path k . $I_{i,j}(k)$ enables fair share of network bandwidth by adjusting the rate of increase in volume based on the total traffic T_i . T_{lim} is the constant fairness coefficient that affects the rate of increase and decrease. When the total amount T_i of traffic derived by Eq. (12) is close to T_{lim} , coefficient $I_{i,j}$ becomes about 0.25 in the unloaded condition. On the other hand, for a session with small T_i , $I_{i,j}$ is about 0.5. On the contrary, in the overloaded condition, $I_{i,j}$ approaches to 0.75 with a large T_i and 0.5 with a small T_i , respectively. Therefore, a smaller session can increase the traffic volume more than a larger session in the unloaded condition and it decreases the traffic volume slower than a larger session in the overloaded condition. Then, we can expect fair share of network bandwidth.

3.2 Implementation of Overlay Multipath Routing

In this section, we explain how the mathematical model proposed in the previous section is implemented in actual overlay networking. First of all, multiple overlay paths must be established among a source node and a destination node of an overlay session. Path establishment can be done by any appropriate methods [17, 18]. In case a reactive method like AODV [19] is used, multiple paths can be found as follows. First a source node

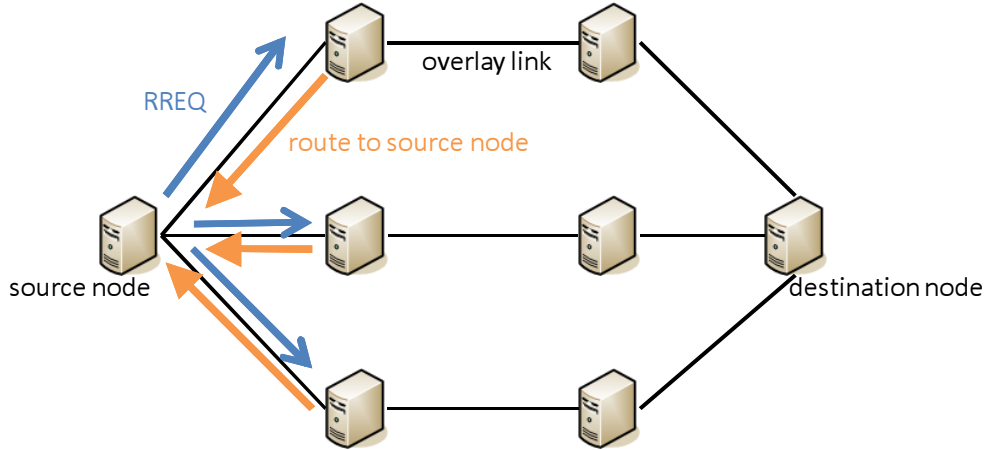


Figure 14: Route setup by RREQ

disseminates RREQ (route request) messages over an overlay network as shown in Fig.14. A RREQ message contains the addresses of the source node and the destination node. When an overlay node receives a RREQ message, it can identify a node from which it first received the RREQ message as the best candidate of the next-hop node for the source node. If the node is not the destination node, it forwards the RREQ message to all of its neighbors except one from which it received the message. As RREQ messages traverse, reverse paths to the source are automatically established (see Fig. 15). Meanwhile, RREQ messages reach the destination node. The destination node generates a RREP (route reply) message and sends it back to a sender of the corresponding RREQ message for each of RREQ messages it receives (Fig. 16). Each RREQ message goes back to the source node by traversing a reverse path of the corresponding RREQ message. Finally, RREP messages reach the source node and at this time paths are established for both direction as shown in Fig.17. It is not necessary for a destination node to answer all RREQ messages that it receives and for a source node to use all paths established. They can limit the number of paths depending on application's requirements and the quality of paths.

Once multiple paths are established, a source node begins to send traffic, i.e. messages to a destination node. Initially, the number L_i of micro traffic of session i is set at 10 and their initial volume $v_{i,j}$ at 0.01. Here, volume $v_{i,j}$ corresponds to the size of data to send or the sending rate. Therefore, the total data size to send at a time or the sending rate

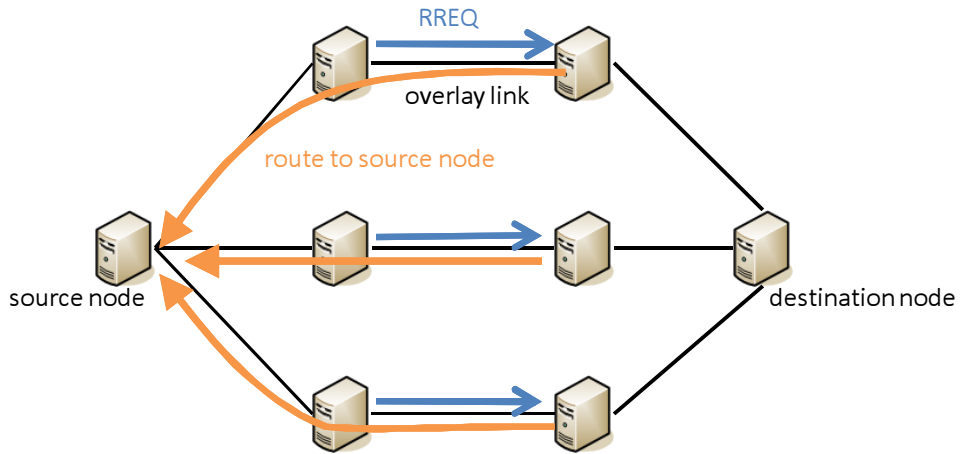


Figure 15: RREQ forwarding

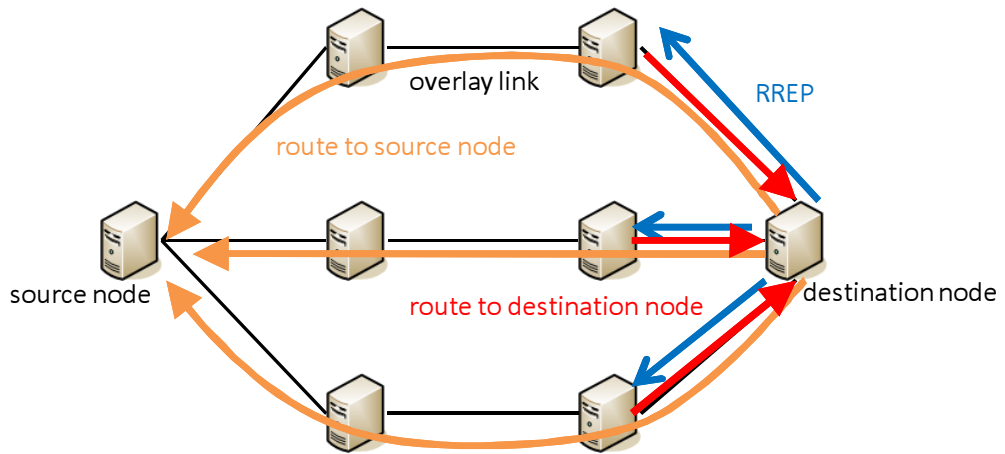


Figure 16: Replaying RREP by destination node

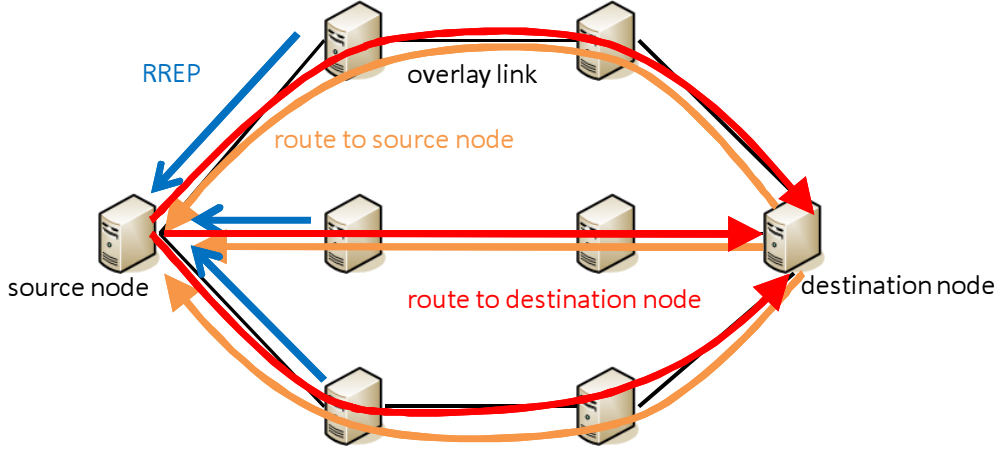


Figure 17: RREP forwarding

of the session is given by T_i . The initial activity $\mu_{i,j}$ is set at 0. By using Eq. (14), the source node obtains the utilization ratio $x_{i,j}(k)$ of each path k . Then, it distributes traffic, i.e. data or messages, to paths in proportional to $\frac{x_{i,j}(k)}{\sum_{l=1}^{M_i} x_{i,j}(l)}$. At regular intervals, the source node probes the load of paths to obtain $\rho_i(k)$. For this purpose, the source node uses such a method in [14], [20]. With the method used in [14], the source node sends probe packets with the timestamp to the destination node and the destination node sends back acknowledgement packets indicating the timestamp of the corresponding probe packet. Then, the source node can estimate the round-trip delay of the path which can be used as an indicator of the load. Another approach is to obtain information about the condition of physical network with a help of physical network itself like P4P [21]. With the measured or obtained information on load $\rho_i(k)$, all of activity $\mu_{i,j}$, utilization ratio $x_{i,j}(k)$, volume $v_{i,j}$ of micro traffic, and total traffic volume T_i . It means that the source node does not only adjust the distribution of traffic but also regulate the amount of traffic, i.e. rate control or congestion control.

By these implementations, traffic in network come to max-min fairness of bandwidth without direct interference between overlay networks. Simulation result which is in case multipath routing in overlay network show Sec. 4.

4 Simulation

In this section, we first see how an overlay session controls traffic adaptively to dynamic changes in the available bandwidth cause by background traffic. Then, we evaluate the fair share of bandwidth with Eq. (16) and then with Eq. (17). Finally, we investigate the effect of parameter T_{lim} .

4.1 Simulation Setting

We conduct simulation experiments in four scenarios. Independently of scenarios, we use the parameter setting summarized in Table 3. In the first scenario, we consider a network topology illustrated in Fig. 19. There is only one overlay session and there are three disjoint paths, i.e. $k=3$, between a source node and a destination node. Each of overlay links has the identical capacity of 1. The overlay session uses Eq. (16) in derivation of the volume of micro traffic where the sigmoid coefficient g is set to 2. To evaluate the adaptability of our multipath routing, we introduce background traffic whose amounts dynamically change as shown in Fig. 19. $B(k)$ corresponds to the background traffic traversing path k . In the next section for simulation results, we focus on four micro traffic numbered 1 through 4 among the initial set of micro traffic to see their behavior, in terms of activity $\mu_{1,j}$, volume $v_{1,j}$, and utilization ratio $x_{1,j}(k)$. We also evaluate the adaptive behavior of the overlay session as a whole, by the amount of traffic $T_1(k)$ for each path k and the average activity $\mu = \frac{\sum_j^{L_i} \mu_{1,j}}{L_i}$.

Next the second scenario considers competition among two overlay sessions for link bandwidth. We used the same topology with the same parameters as the first scenario, but there are two overlay sessions which have the overlapping path as shown in Fig. 20. There is no background traffic. Overlay session 1 starts at time 0 and overlay session 2 starts at time 200. We observe the behavior of two micro traffic for each of overlay sessions, in terms of volume $v_{1,1}$, $v_{1,2}$, $v_{2,1}$ and $v_{2,2}$ and utilization ratio $x_{1,1}(k)$, $x_{1,2}(k)$, $x_{1,3}(k)$, and $x_{1,4}(k)$. We also evaluate the amount T_i of total traffic of each overlay session and the amount $T_i(1)$ of traffic of each session on overlay path 0.

Then, in the third scenario, we change the equation from Eq. (16) to Eq. (17) in deriving the volume of micro traffic. We use the same parameters as the second scenario,

Table 3: Parameters (All scenario)

parameter	value
initial number of micro traffic L_i	10
initial volume of miciro traffic $v_{i,j}$	0.01
initial traffic of overlay session T_i	0.1
initial utilization ratio of micro traffic $x_{i,j}(k)$	0.2
initial activity of micro traffic $\mu_{i,j}$	0
capacity of overlay link	1
inhibition degree S	10
mean of $\eta_i(t)$	0
variance of η_i	0.02
load distribution coefficient K	0.3
capacity coefficient $C_i(k)$	0.5

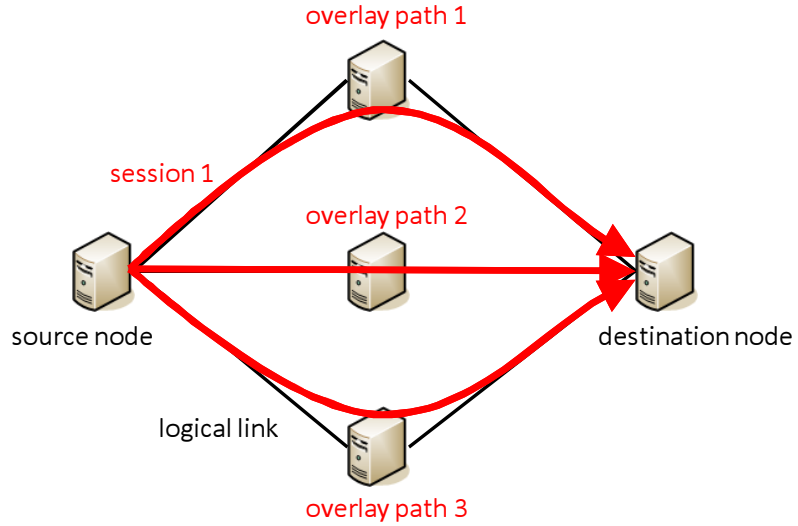


Figure 18: Topology of overlay network (Scenario 1 : single session)

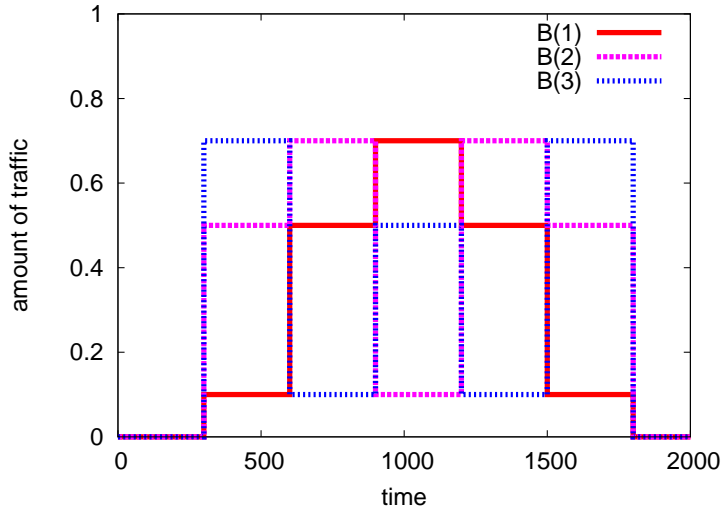


Figure 19: Background traffic (Scenario 1 : single session)

but parameter T_{lim} of 0.1 is used in place of gain g of the sigmoid function.

The third simulation scenario is that we simulate two overlay session competing physical link without background traffic to show that our approach with Eq. (17) achieve max-min fairness. The simulation settings are the same with the second scenario but the equations which determine the dynamics of amount of traffic of overlay session are different between two scenarios where the second scenario uses Eq. (16) and this scenario uses Eq. (17).

Finally, we extend the topology to a larger one with 100 overlay nodes illustrated in Fig. 21. The topology is generated at random. For all pairs of nodes, a link is established at the constant probability. The probability is chosen so that the average degree, i.e. the number of links, becomes five. Then, 10 source-destination pairs are chosen at random allowing a single node to participate in two or more overlay sessions. Parameter setting is summarized in Table 4. To investigate the effect of parameter T_{lim} on the max-min fairness and the convergence time, we change T_{lim} from 0.1 to 5. For each of T_{lim} , we conduct 100 simulation runs with different sets of overlay sessions but on the same overlay network topology. For each of simulation runs, we obtain the average amount \bar{T}_i of session traffic T_i during the last 500 time units. Then, we evaluate the mean square error of the average amount \bar{T}_i of session traffic to the optimal amount $T_{opt,i}$ in the max-min fair share

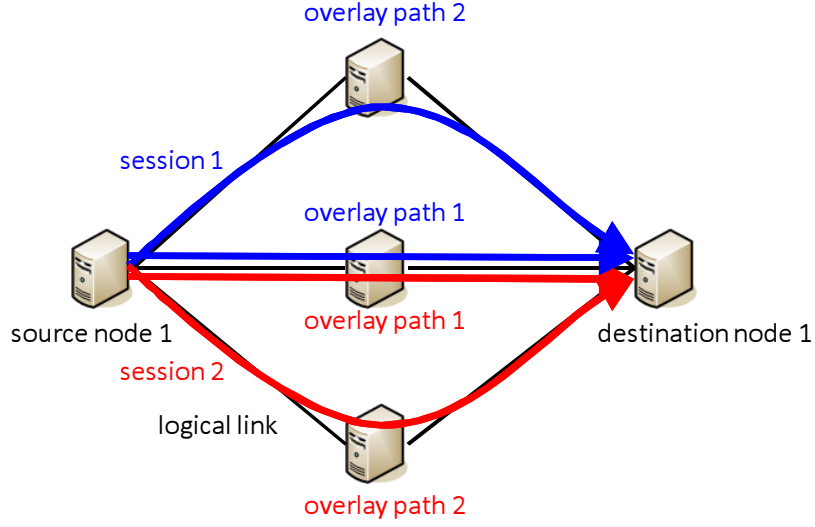


Figure 20: Topology of overlay network (Scenarios 2 and 3 : two sessions)

Table 4: Parameters used in the simulation (Scenario 4 : multiple session)

parameter	value
duration of simulation	2000
fairness coefficient T_{lim}	0.1 to 5 step 0.1

condition, which is derived by a heuristic optimization algorithm.

$$MSE = \sqrt{\frac{\sum_{i=1}^N (\bar{T}_i - T_{opt,i})^2}{N}} \quad (20)$$

where N is the number of overlay session. Because of self-adaptation without any centralized control, it takes time for multipath routing to converge. We regard the time when the degree of change in the average amount T_i of traffic of session i over the last 20 time units becomes smaller than 10 % for all sessions as the convergence time.

4.2 Simulation Results

Results of the first scenario are shown in Figs. 22 through 32. The x-axis of all figures corresponds to simulation time from 0 to 2000 time units. From Figs. 24, 27 and 30, we

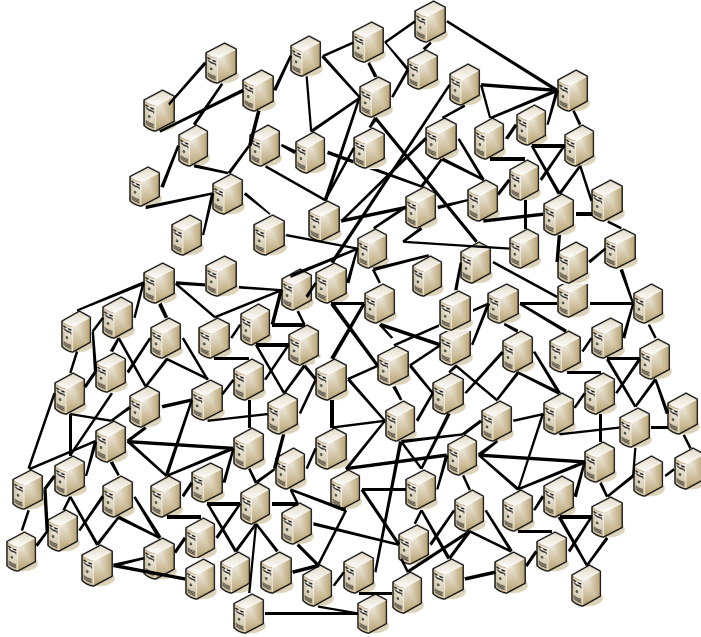


Figure 21: Topology of overlay network (Scenario 4 : multiple session)

can find that micro traffic 1 mainly uses overlay path 1, micro traffic 2 does path 2, micro traffic 3 does path 3.

Initially, activity $\mu_{1,j}$ is small for all micro traffic as shown in Figs. 22, 25 and 28, because there is no traffic in network then all the loads of paths $\rho_i(k)$ are 0. During this period, the noise term in Eq. (14) dominates the dynamics of utilization ratio $x_{1,j}(k)$. Therefore, we see fluctuations in Figs. 24, 27 and 30. At the same time, volume $v_{1,j}$ intensively increases as shown in Figs. 23, 26, 29, because the load of paths $\rho_i(k)$ is lower than the capacity of path 2 then volume $v_{1,j}$ grow slowly. There are two reasons for sudden decrease in the volume of micro traffic. One is for cell division. When the volume reaches 0.02, that is, the twice of initial volume, the micro traffic is divided into two and the volume decreases to the half. The other reason is shrinking for overloading the path. In Eq. (16), the third term of the right-hand side of equation controls the increase or decrease of the volume. When load $\rho_i(k)$ of path k in session i exceeds one, then the right-hand side of equation becomes negative to decrease the volume. As the paths become well utilized, the activity increases following Eq. (14) and each micro traffic eventually chooses one of paths preferentially for entrainment of any one of attractors as Eq. (14) defines. 6

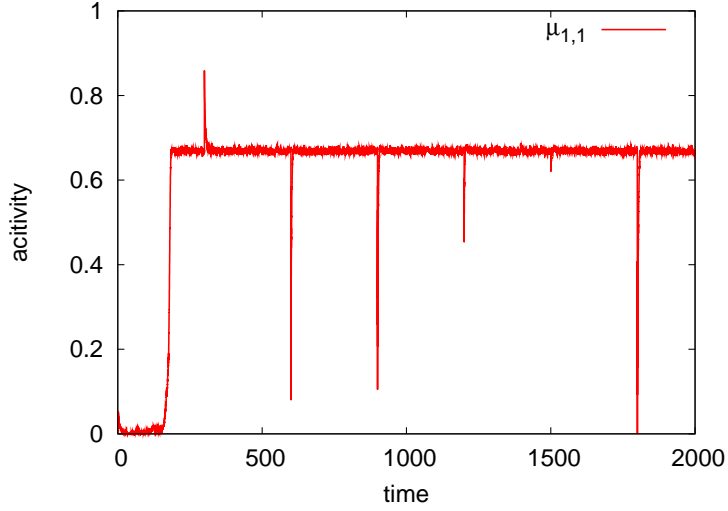


Figure 22: Acvivity of micro traffic 1 (Scenario 1: single session)

Now at time 300, different amounts of background traffic are injected into overlay paths. Background traffic affects load $\rho_1(k)$ of paths and thus the activity changes as shown in figures. The degree of change in the activity depends on the load on the path and the utilization ratio of the path on the session. Therefore, changes in the load of the main path that micro traffic uses does not directly affect the activity. That is why we see spike-shaped changes with various direction and amount in the activity even in the average activity in Fig. 32. Although the activity stays high almost all the time after the initial phase, each micro traffic begins to decrease its volume to suppress the load increased by the background traffic below one by Eq. (16). Consequently, the total traffic $T_1(k)$ of session 1 is regulated to make a room for background traffic as shown in Fig. 31. The total of $B(k)$ and $T_i(k)$ is almost equal to one on all paths. Similarly, the session successfully adapts to changes in the background traffic. A reason that micro traffic 4 changes its main path from 1 to 0 is the effect of noise.

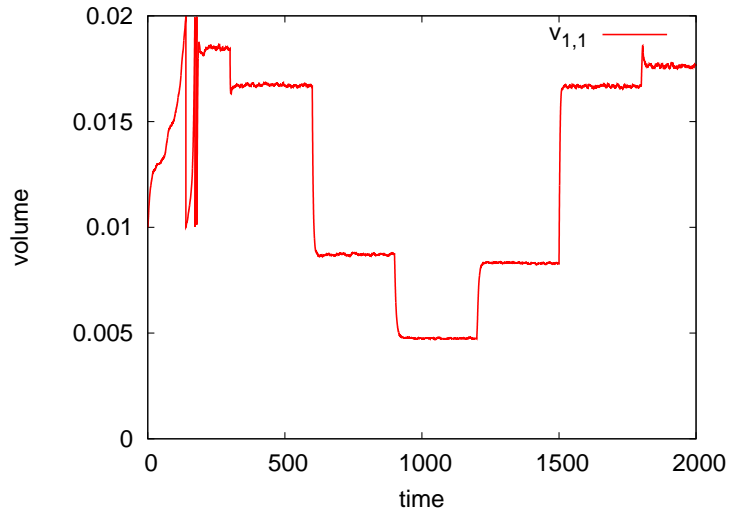


Figure 23: Volume of micro traffic 1 (Scenario 1 : single session)

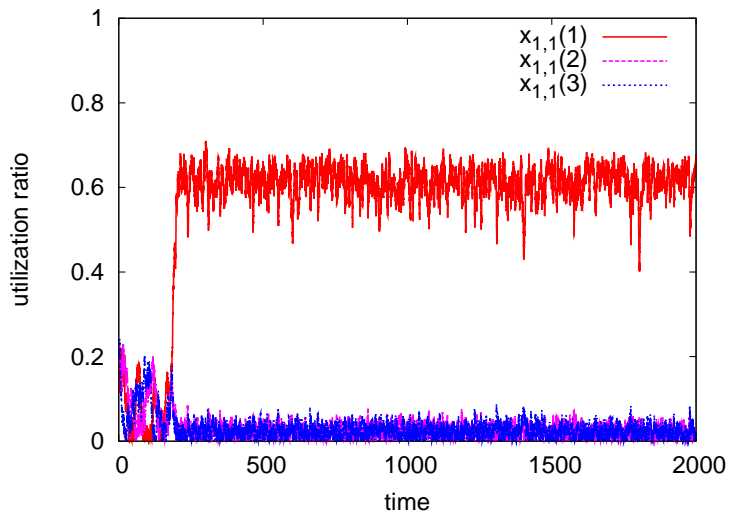


Figure 24: Utilization ratio of micro traffic 1 (Scenario 1 : single session)

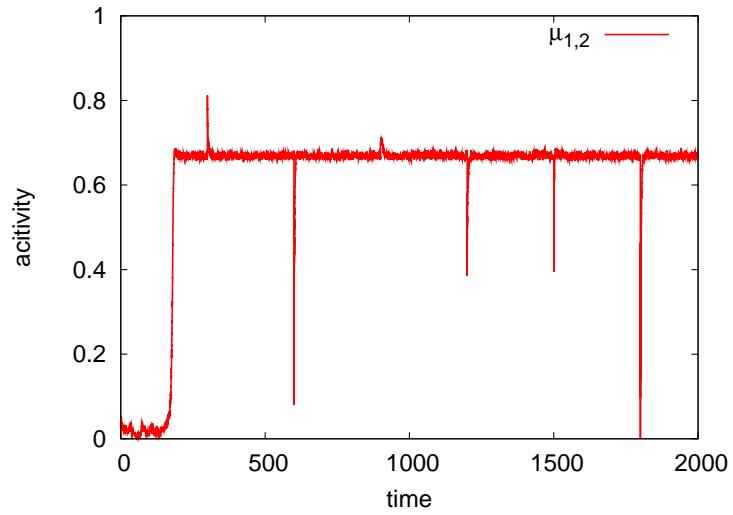


Figure 25: Activity of micro traffic 2 (Scenario 1 : single session)

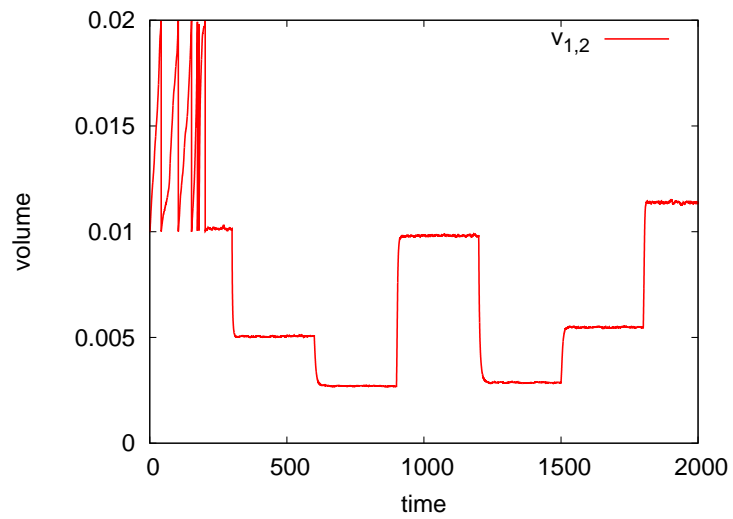


Figure 26: Volume of micro traffic 2 (Scenario 1 : single session)

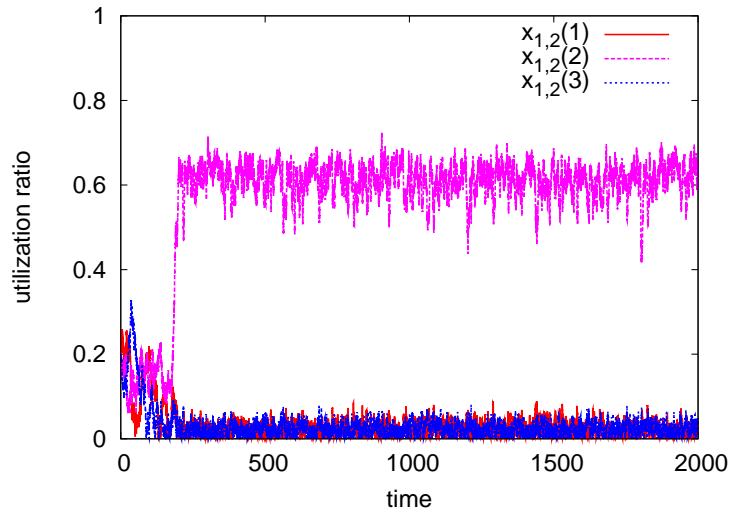


Figure 27: Utilization ratio of micro traffic 2 (Scenario 1 : single session)

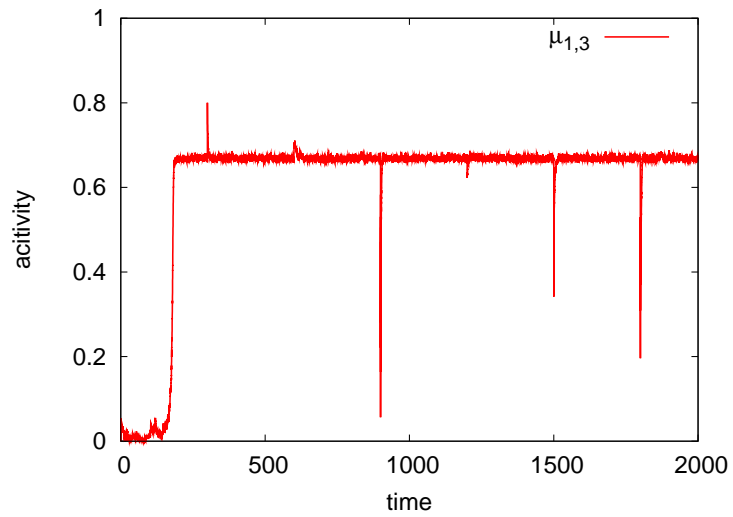


Figure 28: Activity of micro traffic 3 (Scenario 1 : single session)

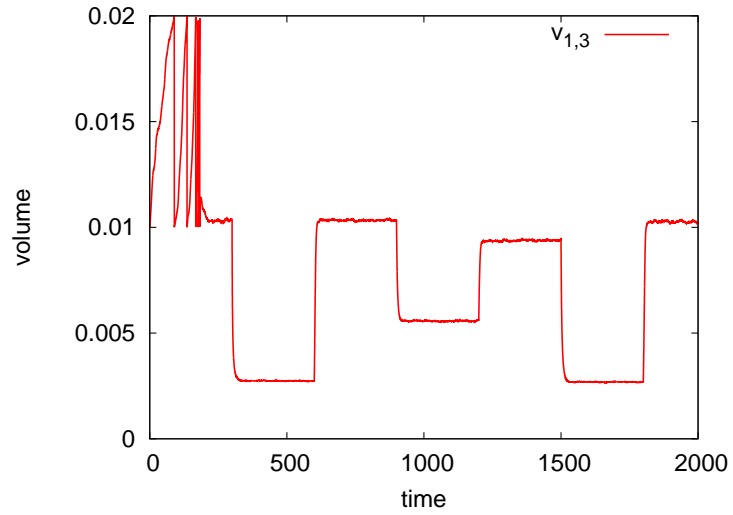


Figure 29: Volume of micro traffic 3 (Scenario 1 : single session)

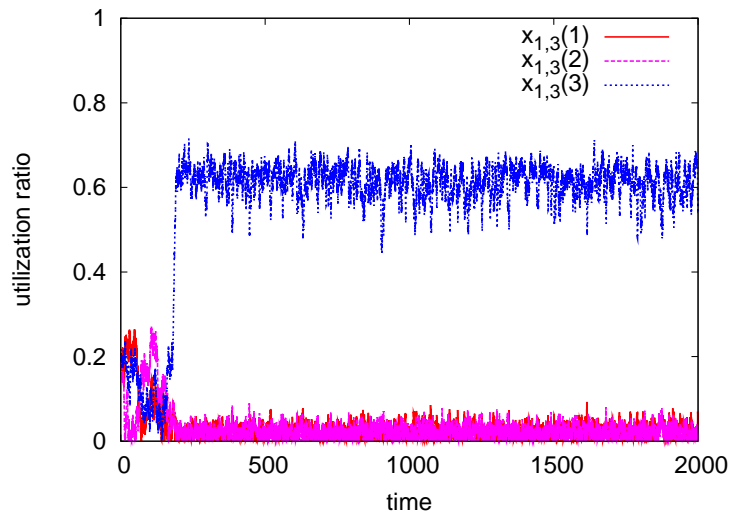


Figure 30: Utilization ratio of micro traffic 3 (Scenario 1 : single session)

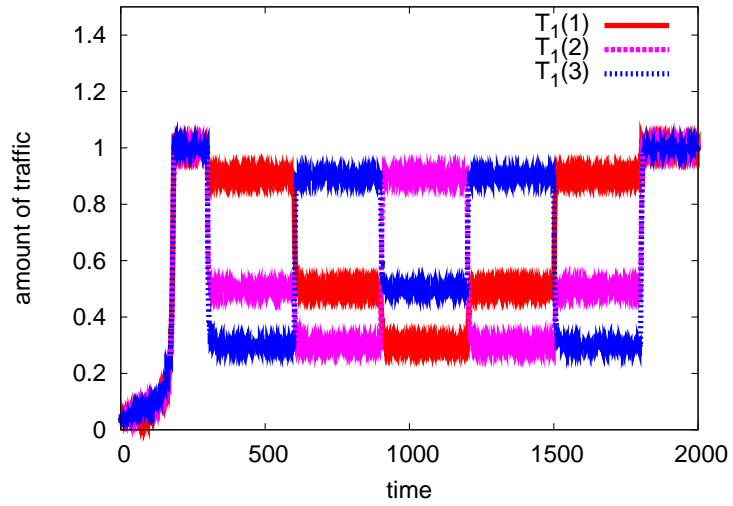


Figure 31: Amount of traffic of overlay session (Scenario 1 : single session)

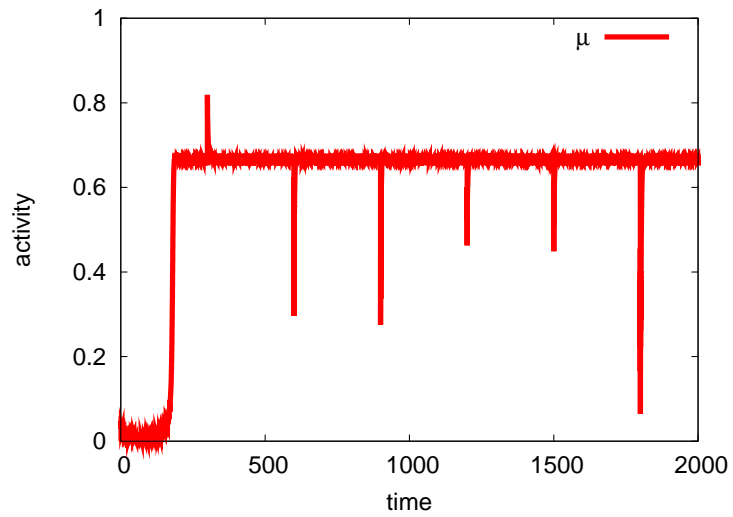


Figure 32: Activity of overlay session (Scenario 1 : single session)

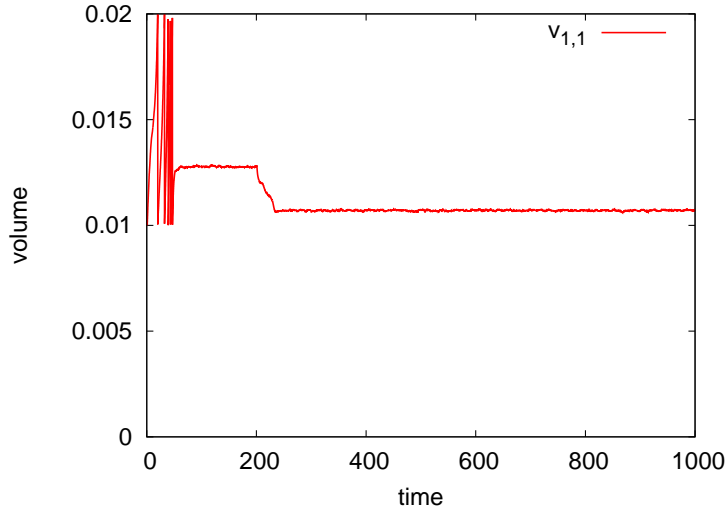


Figure 33: Volume of micro traffic 1 of overlay session 1 (Scenario 2 : two sessions)

Results of the second scenario are shown in Figs. 33 through 42. There are two sessions 1 and 2 and we focus on two micro traffic 1 and 2 of each of sessions. Micro traffic 1 of both sessions mainly uses path 1, which is shared among sessions, and micro traffic 2 of both sessions mainly uses path 2, which is independent from the other session, as shown in Figs. 34, 36, 38, and 40. Although there is slight perturbation at the beginning, volume of micro traffic is kept constant on session 1 as can be seen in Figs. 33 and 35. On the other hand, micro traffic 2 of session 2 also could increase the volume to the certain amount and keep it (see Fig. 39). However, Fig. 37 shows that volume $v_{2,1}$ of micro traffic 1 of session 2, which share the same path with micro traffic 1 of session 1, first increases but drastically decreases to about zero. This implies that the capacity of path 1 is occupied by session 1. Figure 41 shows this fact. The amount $T_1(1)$ of traffic of session 1 on path 1 slightly decreases at time 200, but 83 % of capacity is dominated by session 1. Because of this, the total traffic T_i is also different among sessions as shown in Fig. 42. From the above results, we can conclude that overlay multipath routing with Eq. (16) cannot accomplish the max-min fairness.

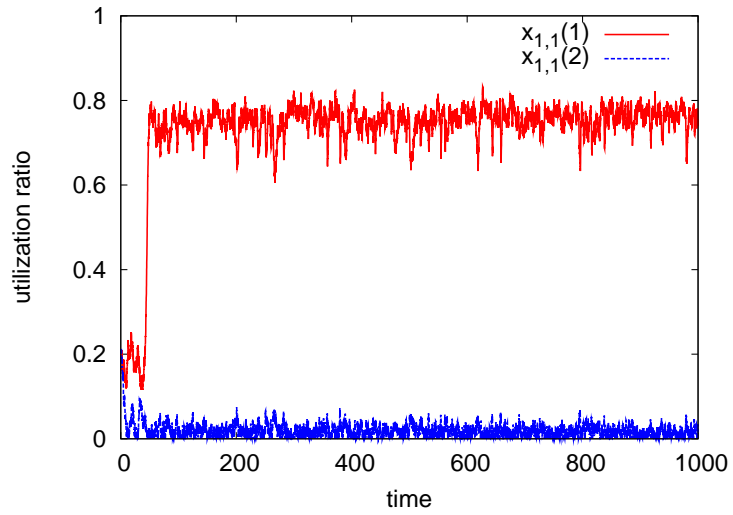


Figure 34: Utilization ratio of micro traffic 1 of overlay session 1 (Scenario 2 : two sessions)

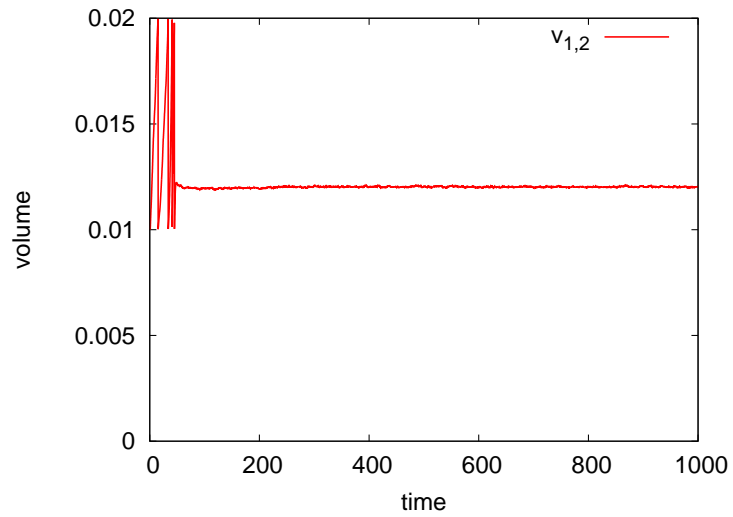


Figure 35: Volume of micro traffic 2 of overlay session 1 (Scenario 2 : two sessions)

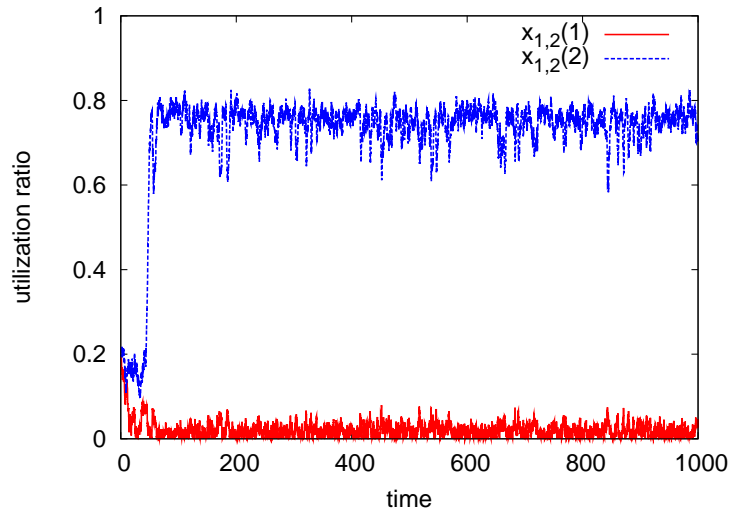


Figure 36: Utilization ratio of micro traffic 2 of overlay session 1 (Scenario 2 : two sessions)

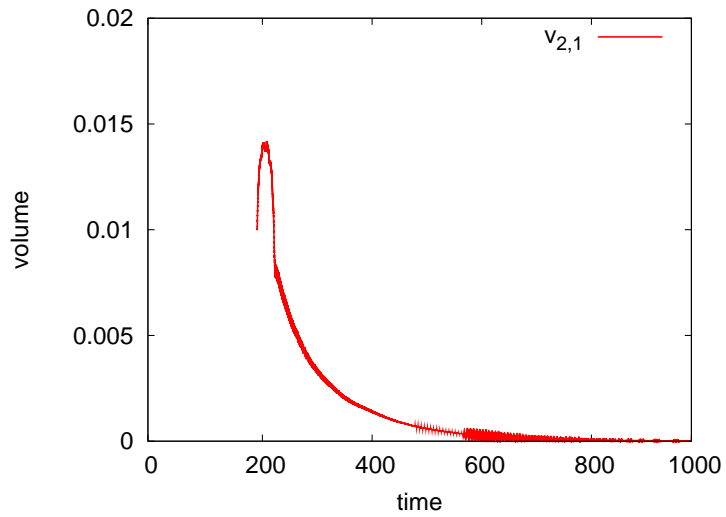


Figure 37: Volume of micro traffic 1 of overlay session 2 (Scenario 2 : two sessions)

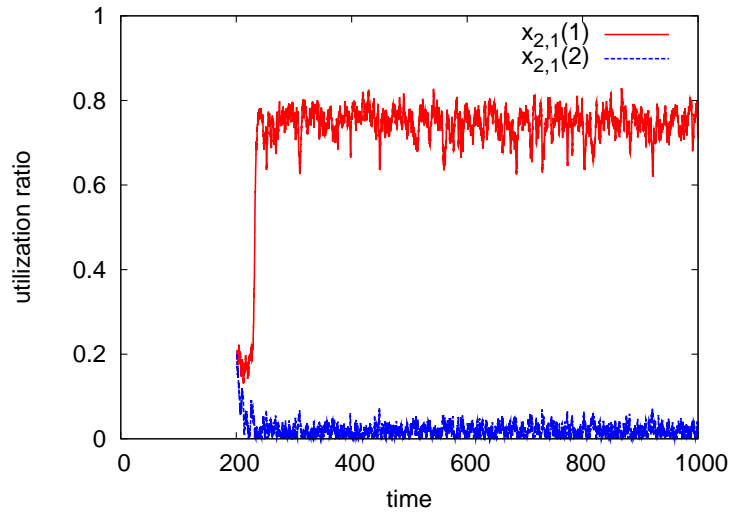


Figure 38: Utilization ratio of micro traffic 1 of overlay session 2 (Scenario 2 : two sessions)

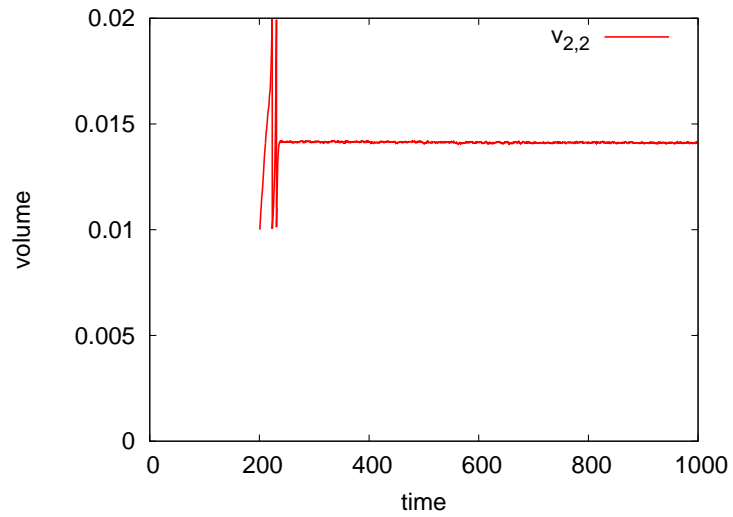


Figure 39: Volume of micro traffic 2 of overlay session 2 (Scenario 2 : two sessions)

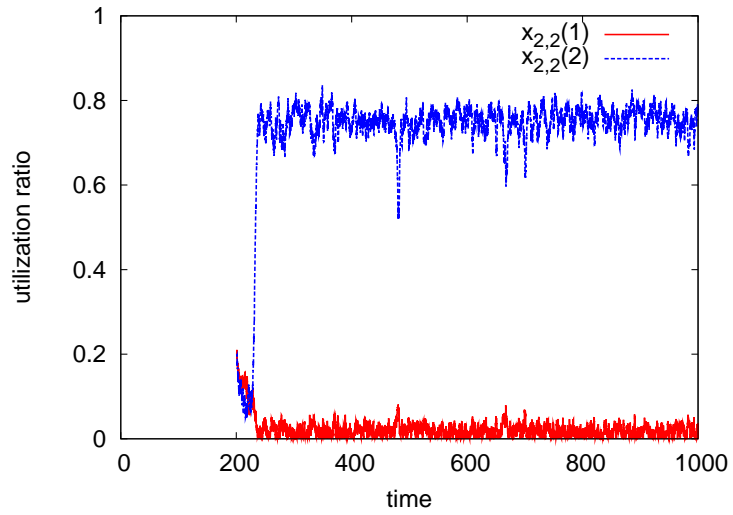


Figure 40: Utilization ratio of micro traffic 2 of overlay session 2 (Scenario 2 : two sessions)

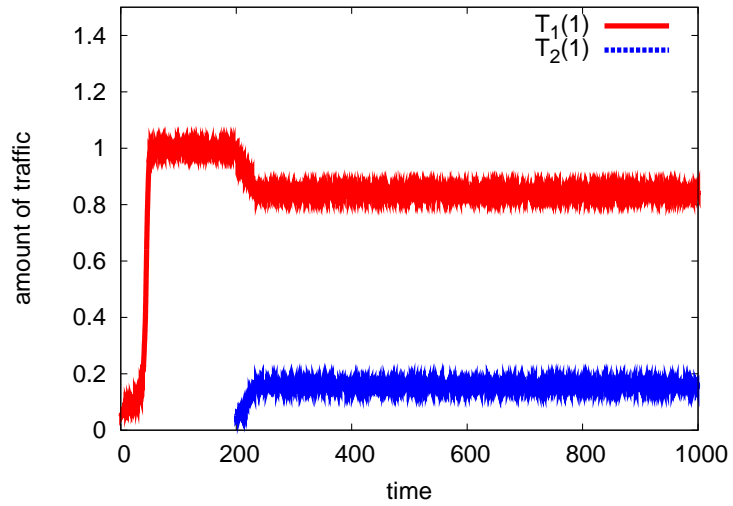


Figure 41: Amount of traffic on overlay path 1 (Scenario 2 : two sessions)

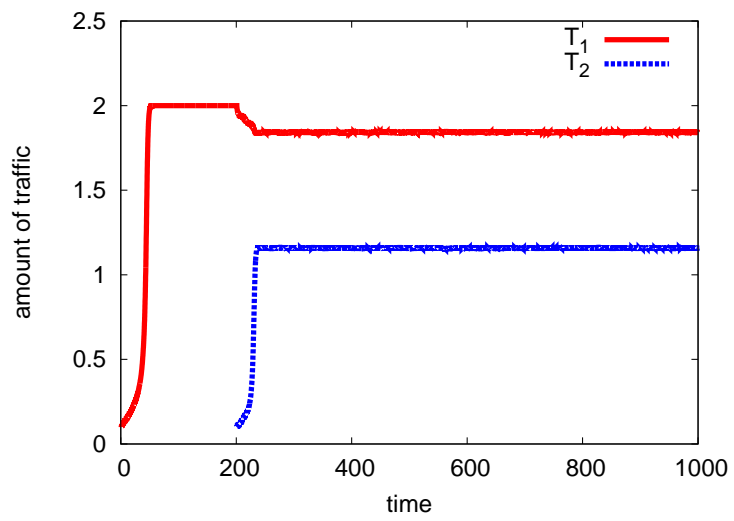


Figure 42: Amount of traffic of each overlay sessions (Scenario 2 : two sessions)

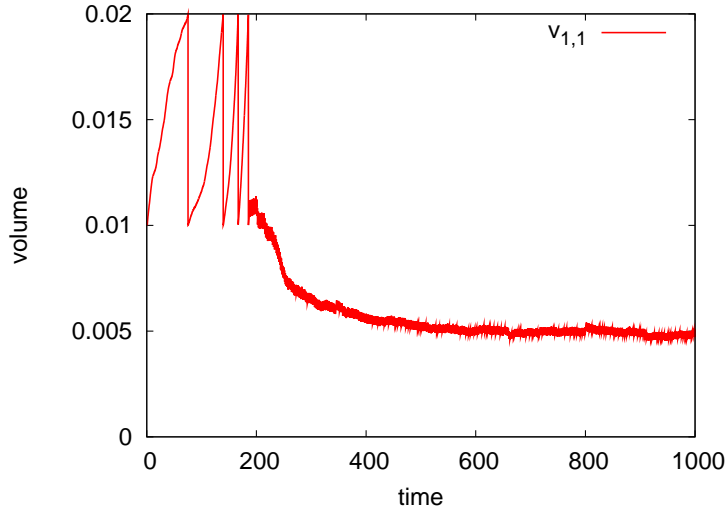


Figure 43: Volume of micro traffic 1 of overlay session 1 (Scenario 3 : two sessions)

In the third scenario, we change the dynamics of traffic volume from Eq. (16) to Eq. (17). All of settings are the same as the second scenario except for this change. Figures 43 through 50 show obtained results. As in the case of scenario 2, micro traffic 1 of both sessions compete for path 1 as shown in Figs. 44, 46, 48, and 50. By using Eq. (17), we make the degree of adaptation more for a session with more traffic. Then, we can accomplish fair share of path bandwidth. In comparing Fig. 33 and Fig. 43, we can see that micro traffic 1 in the latter decrease the volume more intensively than the former, whereas direct comparison is not possible. Consequently, micro traffic 1 of session 2 could successfully increase the volume as shown in Fig. 48, which is considerably different from Fig. 38. Figure 51 shows how two overlay sessions fairly share the bandwidth of competing path. When we look at the total amount of traffic in Fig. 52, it is almost identical among two overlay sessions. Therefore, we can conclude that our multipath overlay routing can accomplish the fair-share of bandwidth in a small scale network.

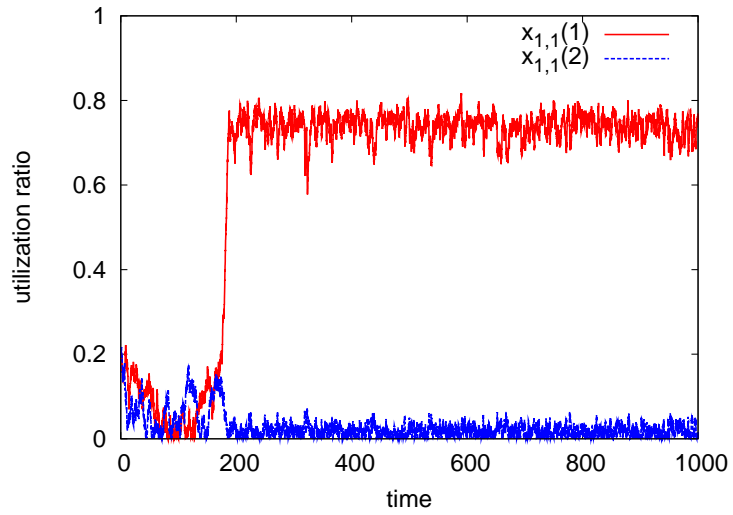


Figure 44: Utilization ratio of micro traffic 1 of overlay session 1 (Scenario 3 : two sessions)

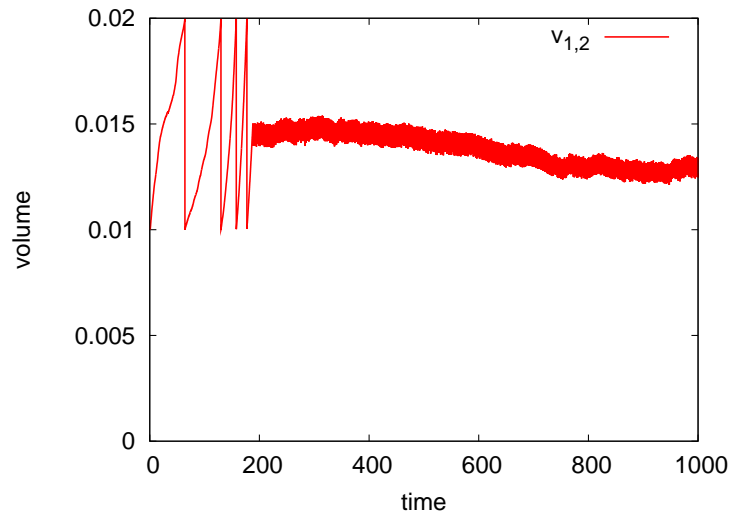


Figure 45: Volume of micro traffic 2 of overlay session 1 (Scenario 3 : two sessions)

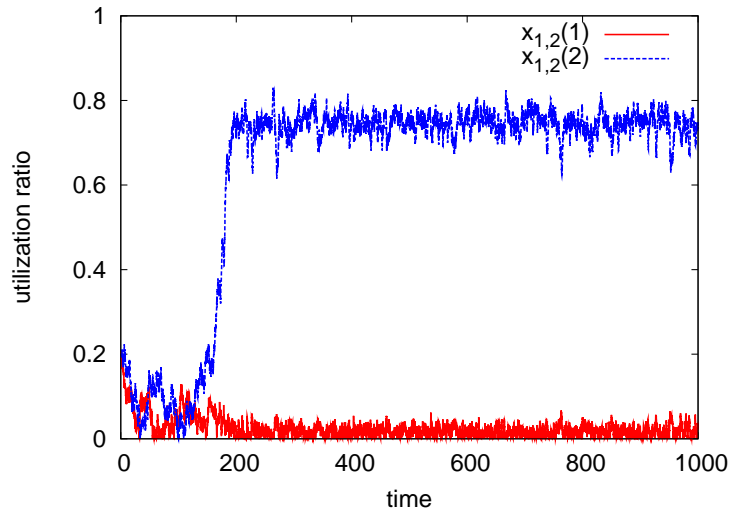


Figure 46: Utilization ratio of micro traffic 2 of overlay session 1 (Scenario 3 : two sessions)

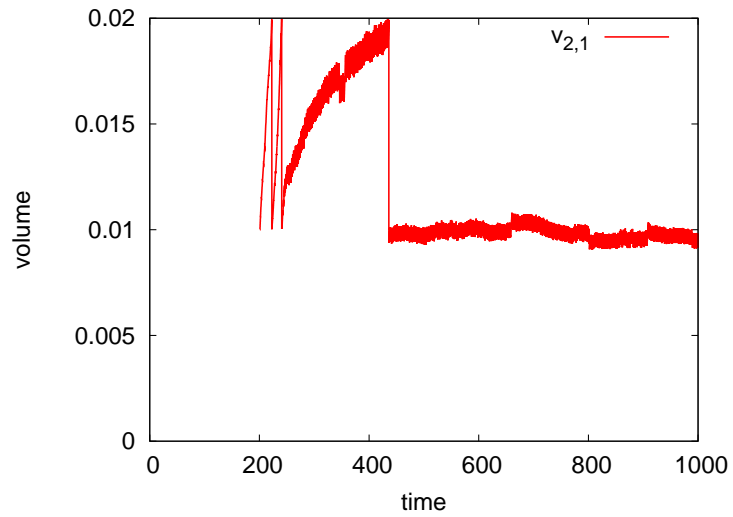


Figure 47: Volume of micro traffic 1 of overlay session 2 (Scenario 3 : two sessions)

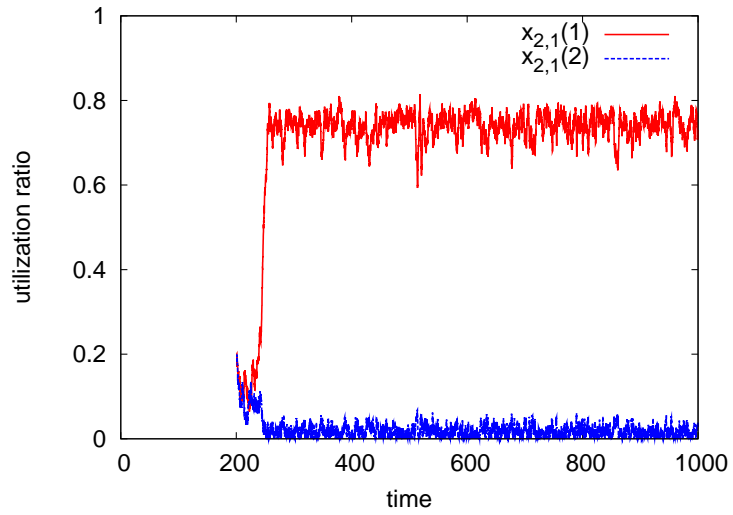


Figure 48: Utilization ratio of micro traffic 1 of overlay session 2 (Scenario 3 : two sessions)

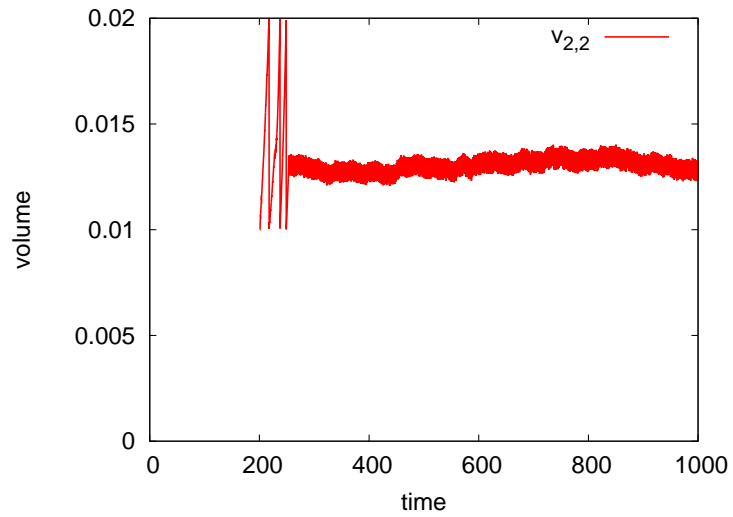


Figure 49: Volume of micro traffic 2 of overlay session 2 (Scenario 3 : two sessions)

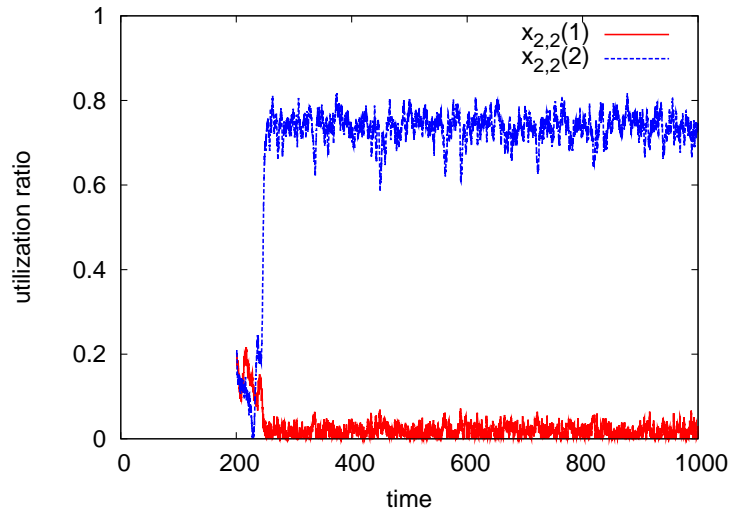


Figure 50: Utilization ratio of micro traffic 2 of overlay session 2 (Scenario 3 : two sessions)

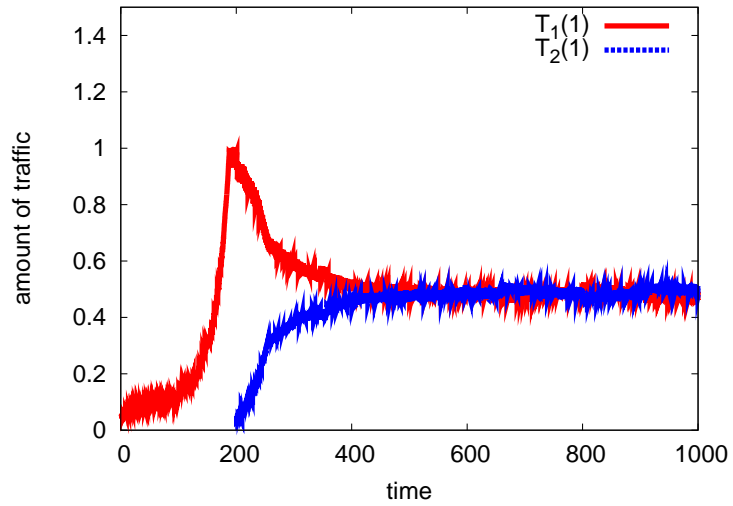


Figure 51: Amount of traffic on overlay path 0 (Scenario 3 : two sessions)

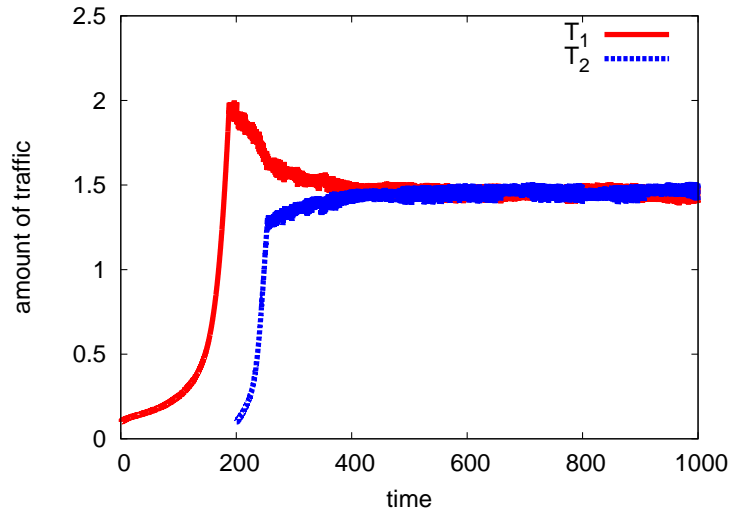


Figure 52: Amount of traffic of each overlay sessions (Scenario 3 : two sessions)

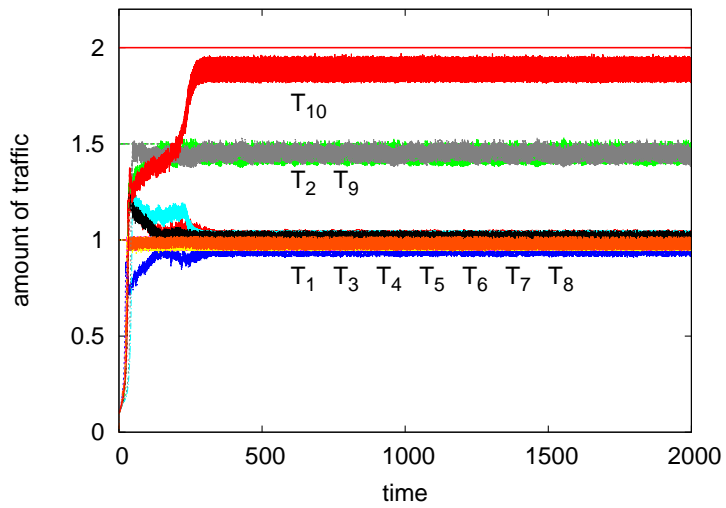


Figure 53: Amount of total traffic of each overlay session (Scenario4 : 10 sessions)

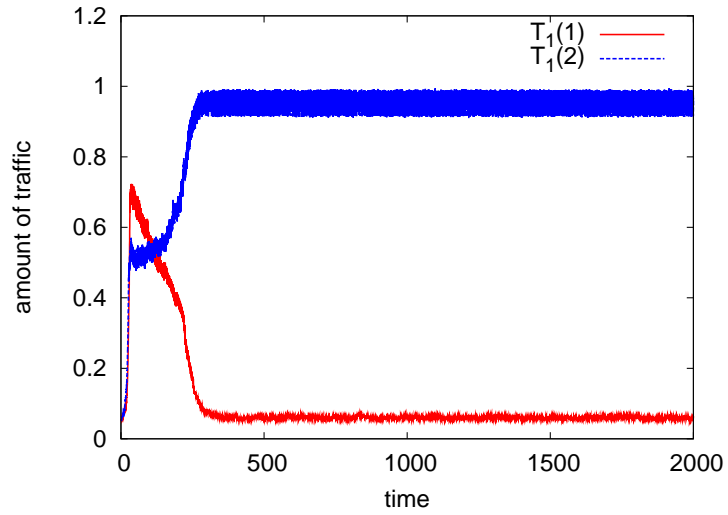


Figure 54: Amount of traffic of overlay sessions 1 (Scenario4 : 10 sessions)

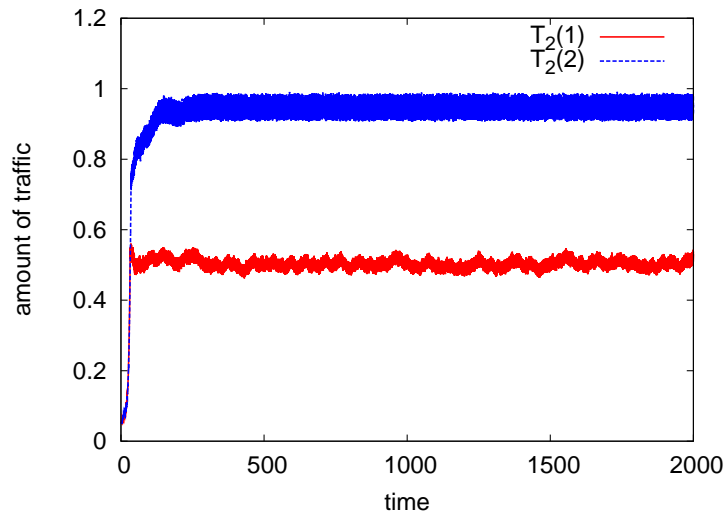


Figure 55: Amount of traffic of overlay sessions 2 (Scenario4 : 10 sessions)

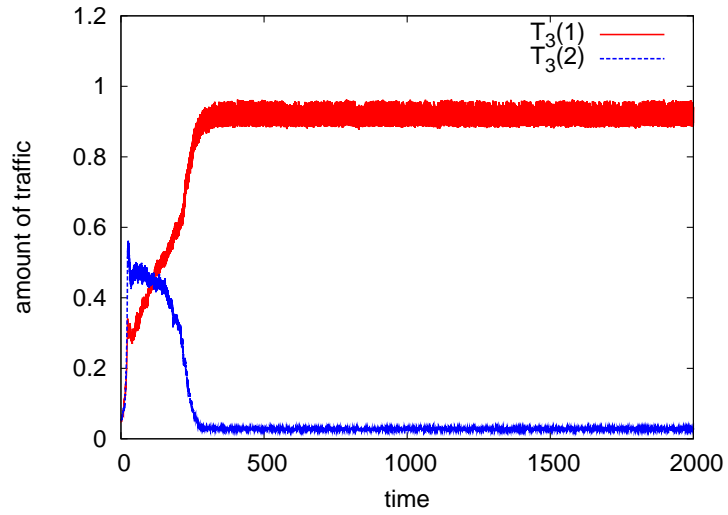


Figure 56: Amount of traffic of overlay sessions 3 (Scenario4 : 10 sessions)

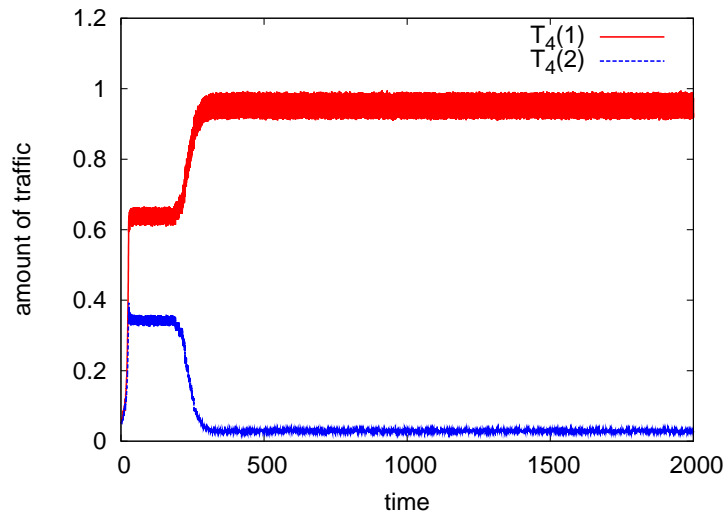


Figure 57: Amount of traffic of overlay sessions 4 (Scenario4 : 10 sessions)

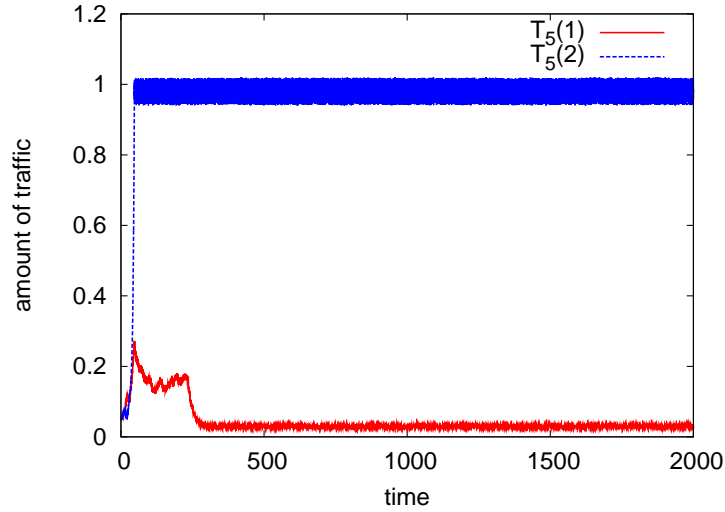


Figure 58: Amount of traffic of overlay sessions 5 (Scenario4 : 10 sessions)

Finally, we show results of the fourth scenario, where 10 overlay sessions co-exist in an overlay network of 100 nodes. Figure 53 summarizes the total amount T_i of traffic of session i for all 10 sessions. The fairness coefficient T_{lim} is set at 1. Figures 54 through 63 show the per-path traffic $T_i(k)$ for each of 10 sessions for reference. In this example, under the condition that the max-min fairness is satisfied, the optimal value of T_i is 2 for session 10, 1.5 for sessions 2 and 9, and 1 for sessions 1, 3, 4, 5, 6, 7, and 8. From Fig. 53, we can prove that our overlay multipath routing can accomplish the max-min fair share of network bandwidth among competing overlay networks in an autonomous and self-adaptive manner. Table 5 summarizes the averages of T_i in the last 500 time units together with the optimal amount derived by the optimization algorithm. We can see that the difference is very small and the MSE of this case is as much as 0.0464.

As explained in section 3.1, the coefficient T_{lim} affects the fairness in our model. Therefore, in Figs. 64 and 65, we change T_{lim} from 0.1 to 5. Figure 64 shows that the average mean square error increases as T_{lim} becomes larger. When T_{lim} is large, the relative effect of the total amount T_i of traffic becomes small by being divided by T_{lim} . Therefore, we cannot compensate the difference in the total amount of traffic by pushing a session of larger traffic to decrease the traffic more aggressively. However, setting T_{lim} too small increase the convergence time as shown in Fig. 64. A reason for this is that a too large

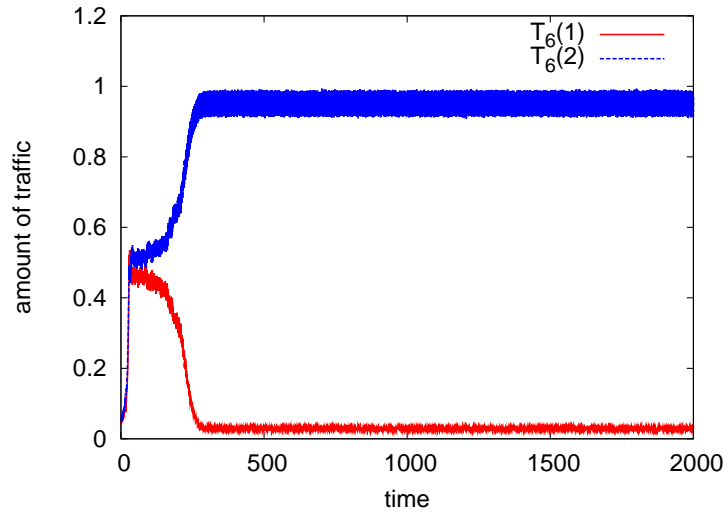


Figure 59: Amount of traffic of overlay sessions 6 (Scenario4 : 10 sessions)

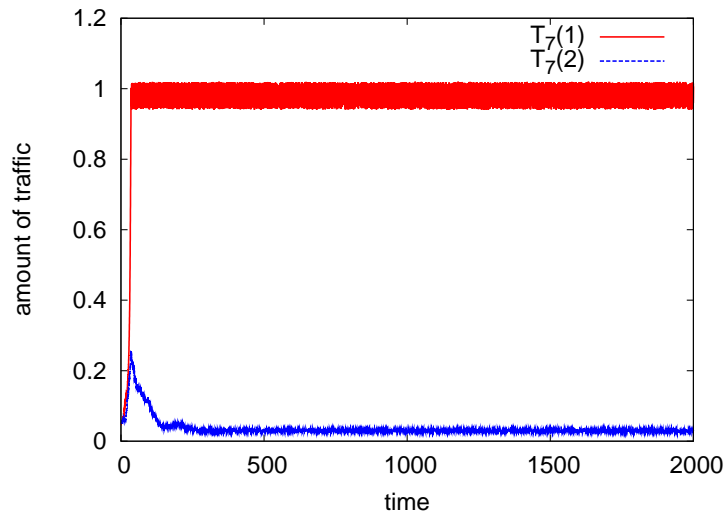


Figure 60: Amount of traffic of overlay sessions 7 (Scenario4 : 10 sessions)

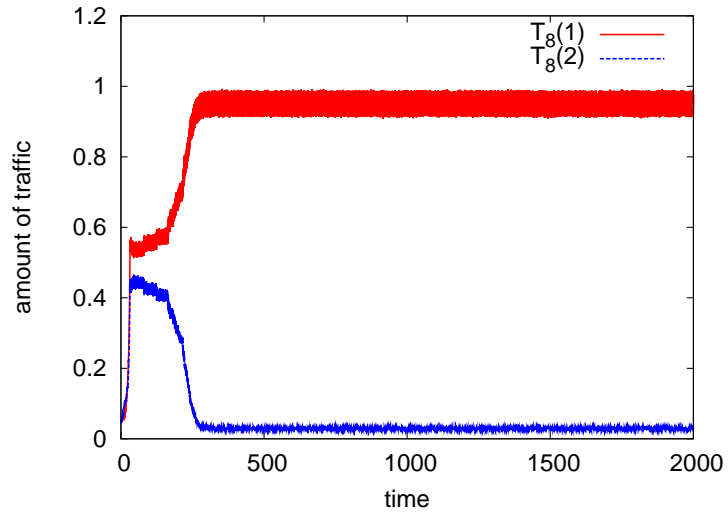


Figure 61: Amount of traffic of overlay sessions 8 (Scenario4 : 10 sessions)

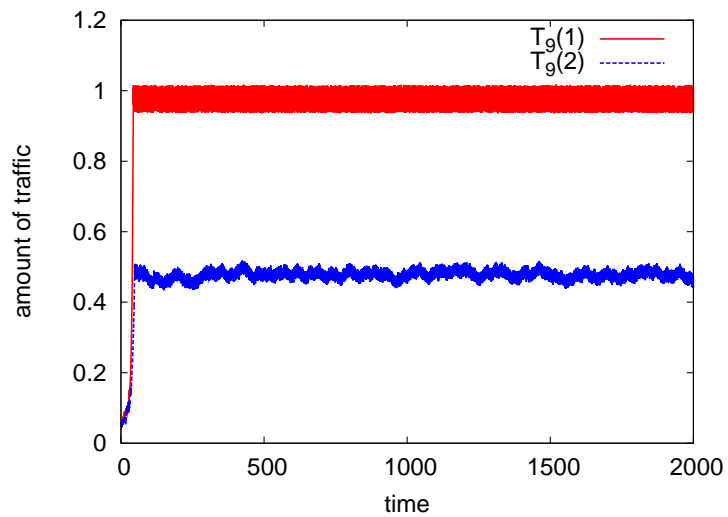


Figure 62: Amount of traffic of overlay sessions 9 (Scenario4 : 10 sessions)

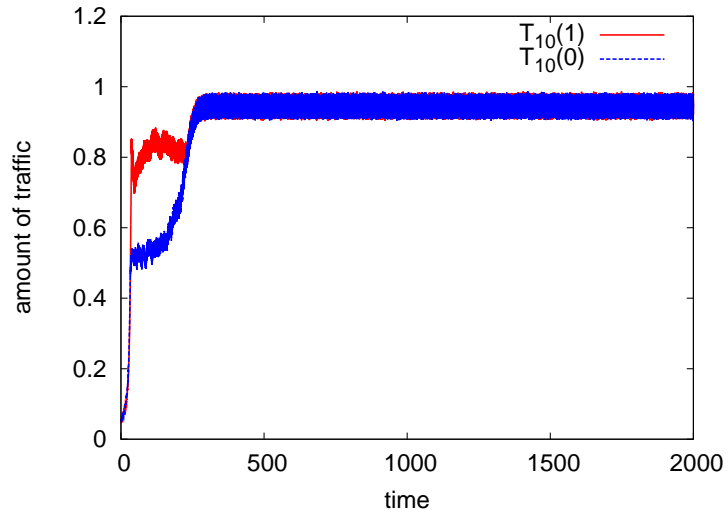


Figure 63: Amount of traffic of overlay sessions 10 (Scenario4 : 10 sessions)

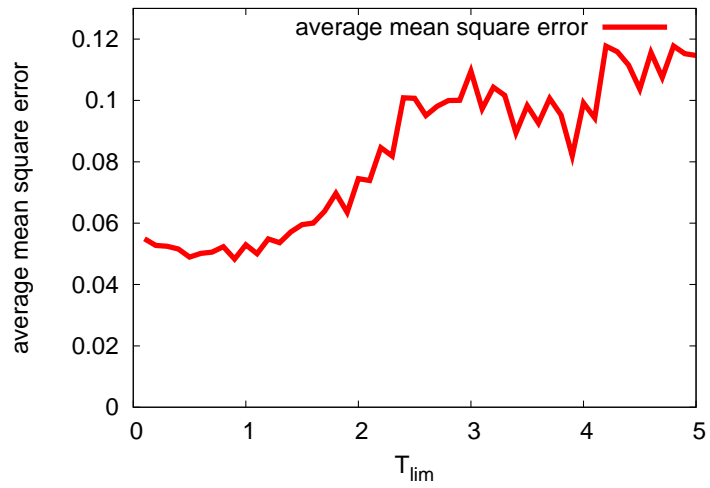


Figure 64: Average MSE against different coefficient T_{lim}

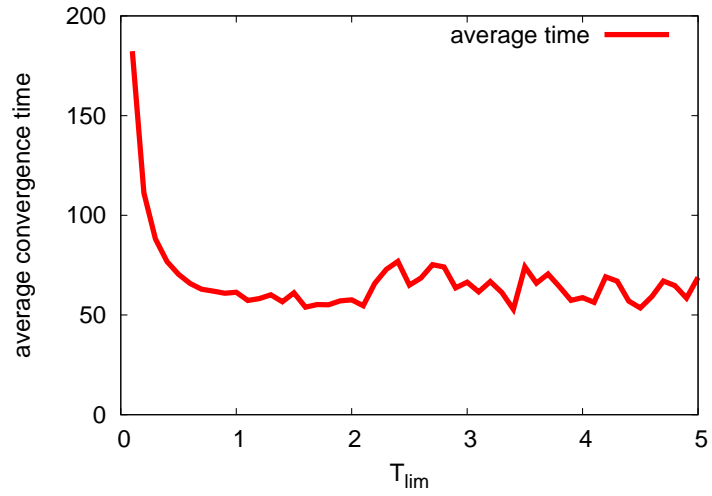


Figure 65: Mean convergence time against different coefficient T_{lim}

T_{lim} makes $I_{i,j}$ in Eq. (19) too small for $\rho_i(k) < 1$. Then, the rate of volume growth becomes small. Consequently, it takes more time for a session to increase the traffic to fully utilize the network bandwidth. From these figures, we can conclude that we should set T_{lim} at around 1 to take trade-off between the max-min fairness and the convergence time.

Table 5: Comparison of average traffic to optimal traffic

session number	average traffic	optimal traffic
1	1.014569	1
2	1.452764	1.5
3	0.946883	1
4	0.979616	1
5	1.011424	1
6	0.979288	1
7	1.010544	1
8	0.978011	1
9	1.451424	1.5
10	1.888865	2

5 Conclusion

In this thesis, we propose a multipath overlay routing mechanism to accomplish the max-min fair share of network bandwidth among competing overlay sessions without a centralized or optimization control. For this purpose, we introduced the extended attractor selection model of adaptive and symbiotic behavior of competing biological systems. Through simulation experiments, we proved that overlay sessions could adaptively adjust the amount of traffic in accordance with dynamically changing load condition and fairly share the network bandwidth in the max-min fair manner.

As future research work, we plan to investigate the influence of control parameters in equations. Although we know that biological systems and their mathematical models in general are insensitive to parameter setting. And they do not need fine tuning of parameters and they should work modestly in a variety of conditions. However, we should confirm this. If a certain level of tuning is necessary, we need to show the baseline of parameter tuning.

Acknowledgements

I get many advices, the opportunities to study many interesting things and more, I express deepest gratitude to Professor Masayuki Murata.

I have very grateful heart for Associate Professor Naoki Wakamiya of Osaka University, for the support I take which enables me to solve a problem and to find good method of thinking.

I am also indebted to Assistant Professors Shinichi Arakawa, Associate Professor Go Hasegawa, Specially Appointed Associate Professor Kenji Leibnitz, Assistant Professor Yuichi Ohsita, Assistant Professor Yoshiaki Taniguchi, Assistant Professor Yuki Koizumi of Osaka University, who gave me helpful comments and feedback.

Furthermore I want to give thanks to all my friends, for the help of research, life, and more.

References

- [1] “Akamai.” <http://www.akamai.com>.
- [2] S. Banerjee, C. Kommareddy, K. Kar, B. Bhattacharjee, and S. Khuller, “Construction of an efficient overlay multicast infrastructure for real-time applications,” in *Proceedings of Twenty-Second Annual Joint Conference of the IEEE Computer and Communications*, pp. 1521–1531, Mar. 2003.
- [3] S. Savage, A. Collins, E. Hoffman, J. Snell, and T. Anderson, “The end-to-end effects of internet path selection,” *ACM SIGCOMM Computer Communication Review*, vol. 29, pp. 289–299, Oct. 1999.
- [4] D. Andersen, H. Balakrishnan, F. Kaashoek, and R. Morris, “Resilient overlay networks,” in *Proceedings of the eighteenth ACM Symposium on Operating Systems Principles*, pp. 131–145, ACM Press New York, NY, USA, Sept. 2001.
- [5] S.-J. Lee, S. Banerjee, P. Sharma, P. Yalagandula, and S. Basu, “Bandwidth-aware routing in overlay networks,” in *Proceedings of The 27th IEEE Conference on Computer Communications*, pp. 1732–1740, Apr. 2008.
- [6] Z. Li and P. Mohapatra, “QRON: QoS-aware routing in overlay networks,” *IEEE Journal on Selected Areas in Communications*, vol. 22, pp. 29–40, Dec. 2004.
- [7] M. Seshadri and R. Katz, “Dynamics of simultaneous overlay network routing,” Tech. Rep. UCB CSD-03-1291, EECS, Nov. 2003.
- [8] L. Qiu, Y. R. Yang, Y. Zhang, and S. Shenker, “On selfish routing in internet-like environments,” in *Proceedings of the 2003 ACM conference on Applications, Technologies, Architectures, and Protocols for Computer Communications*, pp. 151–162, Aug. 2003.
- [9] T. Roughgarden and T. Eva, “How bad is selfish routing?,” *Journal of the ACM*, vol. 49, pp. 236–259, Mar. 2002.

- [10] R. Keralapura, C.-N. Chuah, N. Taft, and G. Iannaccone, “Can coexisting overlays inadvertently step on each other?,” in *Proceedings of 13th IEEE International Conference on Network Protocols*, pp. 203–214, Nov. 2005.
- [11] R. Keralapura, C.-N. Chuah, N. Taft, and G. Iannaccone, “Race conditions in coexisting overlay networks,” *IEEE/ACM Transactions on Networking*, vol. 16, pp. 1–14, Feb. 2008.
- [12] Y. Liu, H. Zhang, W. Gong, and D. Towsley, “On the interaction between overlay routing and traffic engineering,” in *Proceedings of IEEE Conference on Computer Communications*, pp. 2543–2553, Mar. 2005.
- [13] V. Bui and W. Zhu, “A game theoretic framework for multipath optimal data transfer in multiuser overlay networks,” in *Proceedings of IEEE International Conference on Communications*, pp. 401–407, May 2008.
- [14] K. Leibnitz, N. Wakamiya, and M. Murata, “Resilient multi-path routing based on a biological attractor-selection scheme,” in *Proceedings of the Second International Workshop on Biologically Inspired Approaches to Advanced Information Technology*, pp. 48–63, Jan. 2006.
- [15] T. Yomo, W. Xu, and I. Urabe, “Mathematical model allowing the coexistence of closely related competitors at the initial stage of evolution,” *Researches on Population Ecology*, vol. 38, pp. 239–247, Dec. 1996.
- [16] A. Kashiwagi, I. Urabe, K. Kaneko, and T. Yomo, “Adaptive response of a gene network to environmental changes by fitness-induced attractor selection,” *PLoS ONE*, vol. 1, p. e49, Dec. 2006.
- [17] M. Marina and S. Das, “On-demand multipath distance vector routing in ad hoc networks,” in *Proceedings of IEEE International Conference on Network Protocols*, pp. 14–23, 2001.
- [18] R. Ogier and N. Shacham, “A distributed algorithm for finding shortest pairs of disjoint paths,” in *Proceedings of IEEE Conference on Computer Communications*, pp. 73–182, 1989.

- [19] C. Perkins, E. Belding-Royer, and S. Das, “Ad hoc on-demand distance vector (AODV) routing.” RFC 3561 (Experimental), July 2003.
- [20] M. Jain and C. Dovrolis, “Pathload: A measurement tool for end-to-end available bandwidth,” in *Proceedings of Passive and Active Measurements Workshop*, pp. 14–25, Sept. 2002.
- [21] H. Xie, Y. R. Yang, A. Krishnamurthy, Y. Liu, and A. Silberschatz, “P4P: Provider portal for applications,” *SIGCOMM Computer Communication Review*, vol. 38, pp. 351–362, Oct. 2008.